Check for updates

A comprehensive review on MoSe₂ nanostructures with an overview of machine learning techniques for supercapacitor applications

Robertson B,[a] Sapna R,[b] Vinod Hegde[*a] and Hareesh K [ID] [*a]

In the past few decades, supercapacitors (SCs) have emerged as good and reliable energy storage devices due to their impressive power density, better charge–discharge rates, and high cycling stability. The main components of a supercapacitor are its electrode design and composition. Many compositions are tested for electrode preparations, which can provide good performance. Still, research is widely progressing in developing optimum high-performance electrodes. Metal chalcogenides have recently gained a lot of interest for application in supercapacitors due to their intriguing physical and chemical properties, unique crystal structures, tuneable interlayer spacings, broad oxidation states, *etc*. $MoSe_2$, belonging to the family of Transition Metal Dichalcogenides (TMDs), has also been well explored recently for application in supercapacitors due to its similar properties to 2D materials. In this review, we briefly discuss supercapacitors and their classification. Various available synthesis routes for $MoSe_2$ preparation are summarized. A detailed assessment of the electrochemical performances of different $MoSe_2$ composites, including cyclic voltammetry (CV) analysis and galvanostatic charge–discharge (GCD) analysis, is given for symmetric and asymmetric supercapacitors. The limitations of $MoSe_2$ and its composites are mentioned briefly. The use of machine learning methods and algorithms for supercapacitor applications is discussed for forecasting valuable details. Finally, a summary is provided, along with conclusions.

[a]*Department of Physics, Manipal Institute of Technology Bengaluru, Manipal Academy of Higher Education, Manipal 576104, India. E-mail: hegde.vinod@manipal.edu; hareesh.k@manipal.edu*

[b]*Department of Information Technology, Manipal Institute of Technology Bengaluru, Manipal Academy of Higher Education, Manipal 576104, India*

1. Introduction

The energy demands have been unboundedly increasing recently due to the ever-growing population, urbanization, industrialization and technological advancements. As a result, fossil fuels, the primary source of energy, are being depleted

Mr Robertson B received his BSc degree from Bangalore University, India, in 2021 and MSc in Physics from Nrupatunga University, India, in 2023. He is currently pursuing his PhD in the Department of Physics, Manipal Institute of Technology Bengaluru, Manipal Academy of Higher Education, Manipal, India. His research interests include 2D material and nanocomposite-based electrodes for supercapacitors and energy storage applications.

Robertson B

Miss Sapna R is working as an Assistant Professor in the Department of Information Technology, Manipal Institute of Technology Bengaluru, Manipal Academy of Higher Education, Manipal, India. She is currently pursuing her PhD at the Visvesvaraya Technological University. Her areas of interest include Semantic Web, Machine Learning, IoT, Cloud Computing and Green Computing. She has around 7 years of teaching experience. She has published many papers in international journals and international conferences.

Sapna R

rapidly. Excessive use of fossil fuels in automobiles has caused many ecological problems such as air pollution. Other conventional energy sources such as wind energy, solar energy, and hydrothermal energy cannot provide continuous and uninterrupted steady supply of energy. Therefore, there is a need for the search of an alternative energy storage device that is clean, efficient, and sustainable and that can store a considerable amount of energy and provide this energy when required.[1-5] In this context, the development of electrochemical energy storage devices such as capacitors, batteries, fuel cells, and supercapacitors has gained a lot of interest from researchers. Batteries have the disadvantages of poor power density, shorter cycle life, poor power performance, and overheating problems. Conventional capacitors have limited energy density, making them unsuitable for applications requiring long-term energy. SCs, as modern energy storage devices, have been developed to overcome these shortcomings. They are filling the gap between batteries and capacitors because SCs have 100 times better capacitance than normal capacitors. The SCs have impressive power density, quick charging and discharging rates, good cycling stability, and eco-friendliness.[6-9] The development of SCs is important since they can address the future energy storage demands of small portable devices, electric vehicles, smart electronic equipment, hybrid systems, and flexible and wearable device applications.[10-13] A supercapacitor's performance is majorly dependent on the materials of electrodes. Hence, researchers are highly focusing on developing new high-performance electrode materials for SCs for energy storage applications.

Two-dimensional (2D) materials are highly explored for use in supercapacitor electrodes owing to their large surface areas and sheet-like morphologies, which enable the maximum exposure of active sites.[14-18] The 2D material family comprises graphenes, silicene, germanene, borophene, black-phosphorous, hexagonal boron-nitride, MXenes, TMDs, and many others.[19] The evolution of 2D material-based supercapacitor electrodes started from graphene, and later, many
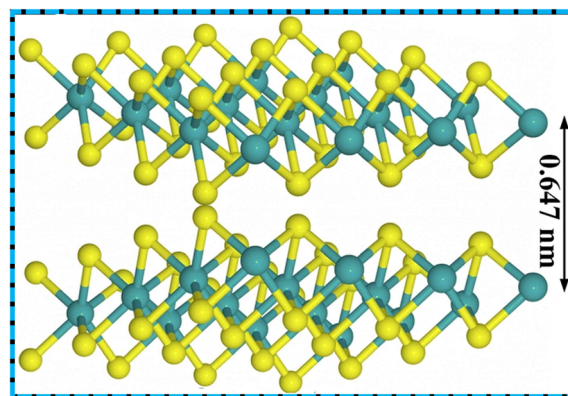

Fig. 1 Three-dimensional view of layers of MoSe$_2$ (Green: Mo, Yellow: Se). This figure has been reproduced from ref. 23 with permission from Springer Nature, Copyright 2018.

other materials in this class were explored further. Recently, TMDs (MoS$_2$, MoSe$_2$, WS$_2$, WSe$_2$, etc.) have attracted considerable attention from researchers to investigate as pseudocapacitive materials for SCs in energy storage and conversion fields.[17] In 2D TMDs, two chalcogen layers (X = S and Se) sandwich a metal layer (M = Mo and W) creating an MX$_2$ structure.[18,20] Among them, MoSe$_2$ has received considerable attention from researchers owing to its graphene-like layered structure, weak van der Waals interactions between the layers, and many other interesting properties. An analog of MoS$_2$, MoSe$_2$, has a layered structure with two Se layers sandwiched by a Mo layer at an interlayer spacing of about 6.5 Å. MoSe$_2$ layers are created by covalently joining the nearby atomic layers, and van der Waals forces stack the adjacent MoSe$_2$ layers into bulk structures.[21,22] Ion intercalation and de-intercalation can occur easily due to the wide interlayer spacing between the layers of MoSe$_2$. Fig. 1 shows the three-dimensional view of MoSe$_2$ layers with a gap of 0.647 nm. Fig. 2 gives the number of research publications on MoSe$_2$ over the past few years. MoSe$_2$ has

Dr Vinod Hegde received his PhD (2021) from Manipal Academy of Higher Education. At present, he is an Assistant Professor of Physics in the Department of Physics, Manipal Institute of Technology Bengaluru, Manipal Academy of Higher Education, Manipal, India. He is doing research on the applications of 2D chalcogenide materials for energy storage and energy conversion applications.

Vinod Hegde

Dr Hareesh K received his PhD (2014) from Mangalore University, India, followed by Post-Doctoral Fellowship (2013–2017) from Savitribai Phule Pune University, India, and University of Western Australia, Australia. Currently, he is an Assistant Professor-Senior Scale in Physics in the Department of Physics, Manipal Institute of Technology Bengaluru, Manipal Academy of Higher Education, Manipal, India. His research interests include the applications of 2D materials in sensing, field emission, supercapacitance, hydrogen production and photovoltaic applications.
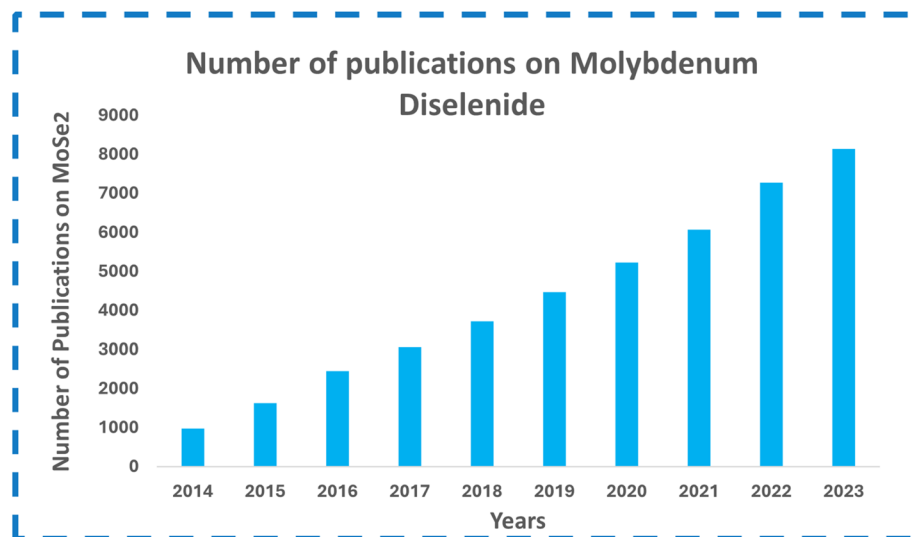
Hareesh K

Fig. 2 Number of publications on $MoSe_2$ electrodes. Compiled from Google Scholar with search "$MoSe_2$".

a better metallic character than MoS_2, and its lower Gibbs free energy promotes its electrochemical activity in catalytic applications.[24] $MoSe_2$ has a better intrinsic electrical conductivity than that of MoS_2 due to the better metallic nature of Se than that of S, making it an intriguing narrow-band-gap semiconductor with comparable layered structures. Electrolyte ion intercalation is made simple by the wider layer gap (0.647 nm) between two $MoSe_2$ layers compared to other counterparts (*e.g.*, graphite has 0.335 nm, and for MoS_2, its 0.615 nm). Low internal resistance and high faradaic capacitance are made possible by the unsaturated Se stable edge structure and the ability to provide many electrochemically active sites.[25] Two distinct symmetry types are present in $MoSe_2$ (1T octahedral and 2H trigonal prismatic). The 1T phase is metallic in contrast to the semiconducting 2H phase. Because of its thermodynamic instability, the 1T phase of $MoSe_2$ eventually changes into the 2H phase.[22,26] All these interesting properties have made $MoSe_2$ gain research interests for SCs. Nevertheless, the specific capacitance of $MoSe_2$ is still too low to be utilized in its pure form for energy storage applications, and its electrical conductivity is still lower than that of carbon materials such as graphenes. Numerous researchers have created a variety of $MoSe_2$-based nanocomposites including graphenes, carbon aerogels, carbon nanotubes, and polyaniline, to address these shortcomings. Compared to pure $MoSe_2$, electrochemical experiments have shown that the $MoSe_2$-based composites provide outstanding cycling stability and a high specific capacity.

Recently, with the advancement of Machine Learning (ML) in the area of Artificial Intelligence (AI), it has become possible to develop better high-performance electrodes for SCs.[27] Specifically, by using the ML methods, it is now possible to accurately predict the capacitance of the electrode materials,[28] forecast the results without experimentations,[29] provide optimized reaction parameters,[30] estimate the reaction rate,[31] explore new electrode materials,[32] determine remaining useful

life,[33] analyze the state of health,[34] estimate the state of charge[33] and predict the cycling stability[35] as well. This will save a lot of time and effort for the researchers since a lot of details can be gathered from the ML models without performing trial-and-error experiments. For SCs, ML algorithms work on a large set of input data from already published works and results. Using suitable algorithms, the ML models are trained to gather and analyze the extensive input data. The ML models learn to map inputs to outputs by adjusting their parameters based on the training data. After this, the ML model can make decisions based on unseen future data. The ML models can update the new data and work in real time. Various ML models such as Neural Networks, Random Forest, XGBoost, Support Vector Machines, Decision Trees, and Linear Regression are available. By selecting an appropriate model, useful details can be accurately derived for developing supercapacitor electrodes as per the requirements.[36]

Herein, we comprehensively review the $MoSe_2$ and $MoSe_2$-based composite electrodes for supercapacitor applications. The different synthesis routes adopted for the development of $MoSe_2$ are provided. Brief workings of implementing ML models in the field of SC applications for capacitance prediction, remaining useful life determination, *etc.*, are also discussed. Finally, challenges faced by $MoSe_2$-based electrodes and future perspectives are provided along with conclusions.

1.1 Supercapacitor fundamentals

SCs primarily take the form of Electric Double Layer Capacitors (EDLCs), pseudocapacitors and hybrids depending on energy storage techniques. EDLC electrodes store charges electrostatically and not *via* faradaic reactions or charge transfer. A double layer of charges is accumulated on the electrode when voltage is supplied. The diffusion of electrolyte ions occurs towards oppositely charged electrodes. When double layers are formed, this reduces the inter-separation distance, which contributes directly to an increase in capacitance. Here, the recombination

of ions does not take place during double-layer formation. EDLCs have good energy density due to the use of carbon-based electrodes, which have large surface areas, and due to reduction in charge separation distance. EDLCs have good power outputs, fast and quick energy intake, and better energy distribution. Moreover, energy storage mechanisms do not involve any chemical reactions, and they are non-faradaic in nature. Compared with batteries, which have the ability to withstand only a few thousand cycles, EDLCs have the ability to continue for millions of cycles. They have drawbacks of poor power density. Conducting polymers, metal oxides and other pseudocapacitive materials are selected in the case of pseudocapacitors. Here, energy storage is mainly electrochemical in nature. The mechanism of energy storage is dependent on faradaic reactions that occur between electrodes and electrolytes. Faradaic reactions involve quick oxidation and reduction reactions. In EDLCs, no charge transfer occurs, but in this case, charge transfer occurs between electrolytes and electrodes. When a potential is supplied, a faradaic current passes through the SC cell. Compared to EDLCs, pseudocapacitors can store more charges, provide better energy densities, and show increased specific capacitances. They have the disadvantage of low cyclability issues. Recently, hybrid capacitors have become a major class of supercapacitors which include both EDLCs and pseudocapacitors. Here energy is stored both electrostatically (non-faradaic) and electrochemically (faradaic). It combines the best features of EDLCs and pseudocapacitors, overcoming the drawbacks of both types, thereby providing more energy density and better life cycles. Hybrid capacitors can further be grouped into three types depending on the electrode materials and configuration: asymmetric hybrids, composite hybrids, and battery-type hybrids. Composite hybrids consist of two or more materials that are utilized for electrodes. Composites can be binary, ternary, and quaternary. Several examples of composites such as carbon–carbon composites, conducting polymer composites, and carbon–metal oxide composites are available. Utilizing two or more materials may produce a synergistic effect that assists in charge transfer and energy storage. In asymmetric hybrids, both EDLCs and pseudocapacitor materials are used in combination. One electrode will be EDLC in nature, and the other electrode will be pseudocapacitive in nature, thereby utilizing both faradaic and non-faradaic processes. From the CV curves, distinction can be made between capacitive-type, pseudocapacitive-type, EDLC-type, and battery-type behaviors of electrodes. In the battery-type hybrid group, battery-type and SC-type electrodes are used together, thereby bridging the gap between the power density and the energy density.[37–46] Fig. 3 gives the classification of SCs depending on possible materials used. Fig. 4 shows the stages of development of SCs, models for describing EDLC mechanisms, and Ragone plot for comparing available energy storage devices.

The performance of lab-scale prepared electrodes can be tested in three designs, namely three-electrode set-up, symmetric set-up, and asymmetric set-up. The three-electrode system comprises electrolyte, working electrode, reference electrode, and standard electrode. The two-electrode setup (symmetric and asymmetric) has two electrodes made up of highly supercapacitive materials. For symmetric, both electrodes will be based on the same material. For asymmetric, the anode material will be different from the cathode material.
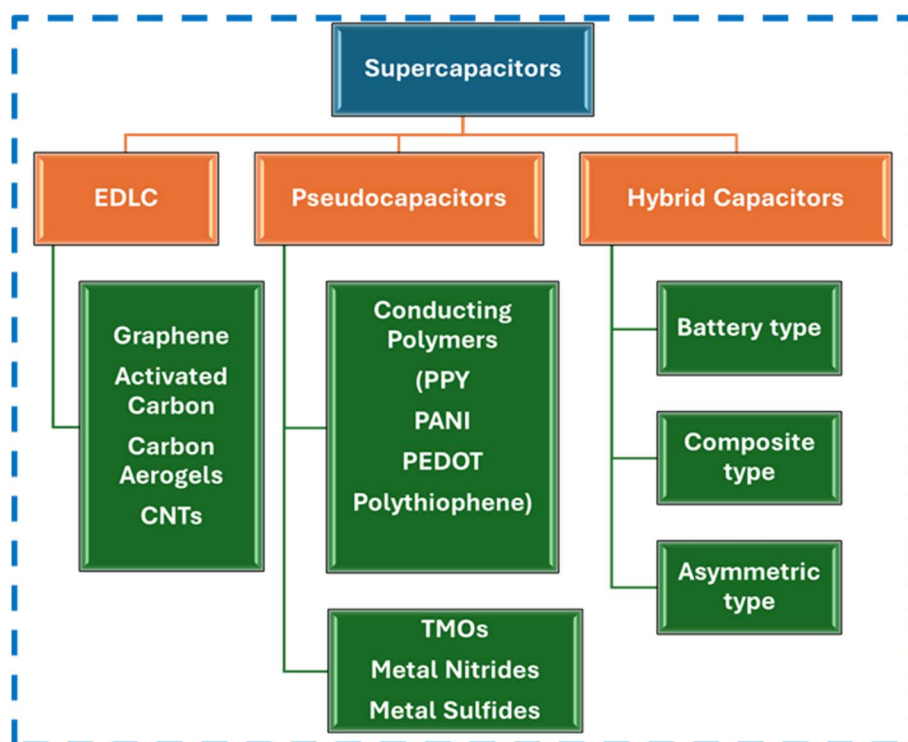

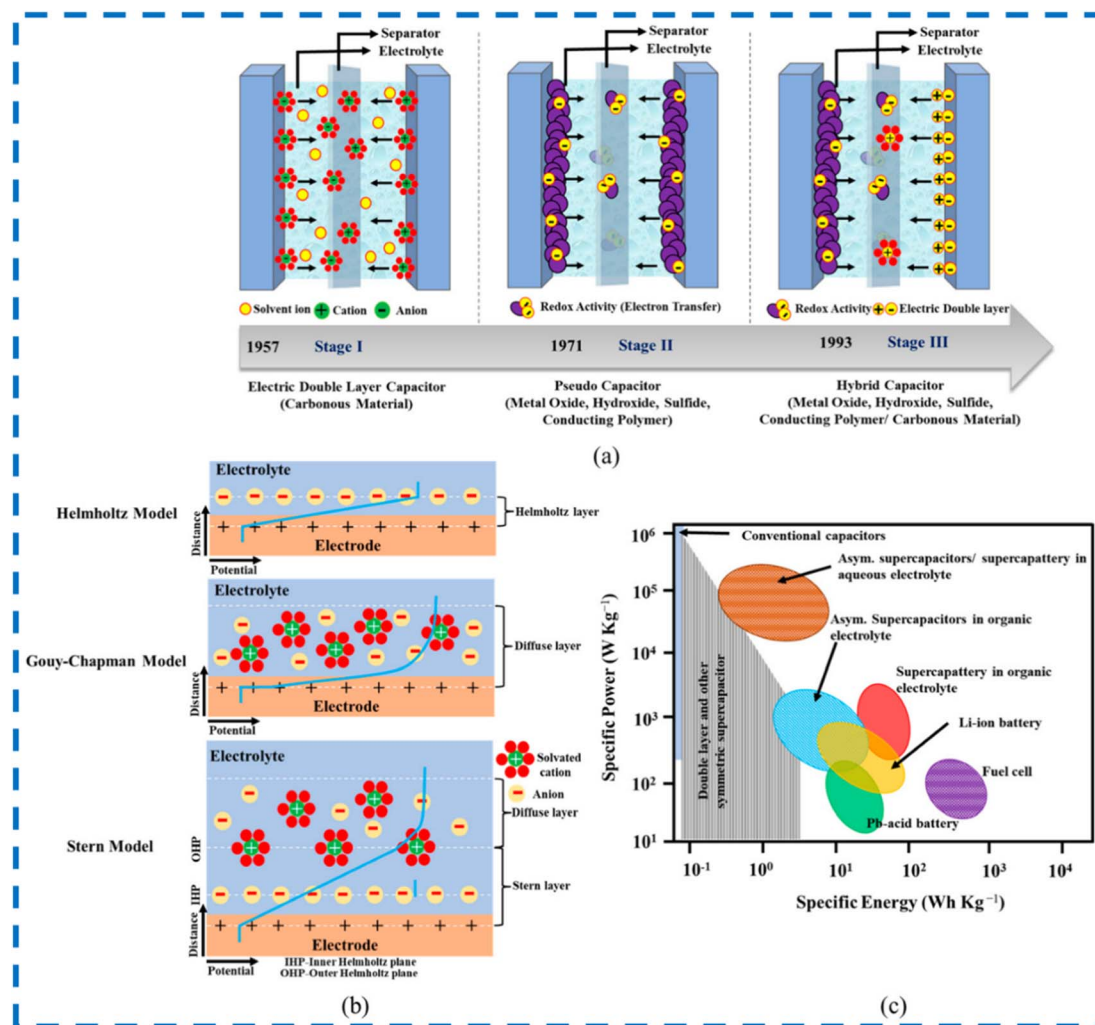Fig. 3 Supercapacitor classification with the possible materials used.

Fig. 4 (a) Classification of supercapacitors. (b) Models for EDLCs. (c) Comparing available energy storage devices. This figure has been reproduced from ref. 47 with permission from MDPI, copyright 2024.

Activated carbon (AC) has been majorly used as one of the asymmetric electrodes in several works. The two-electrode setup provides a better representation of the charge storage performance of the material compared to the three-electrode setup. The most frequently used one is the asymmetric and three-electrode set-up. From the CV curves, for the asymmetric set-up, the specific capacitance can be found using the following equation:

$$C_s = \frac{\int I(V)\mathrm{d}V}{vm\Delta V} \, (\mathrm{F \, g^{-1}})$$

where v stands for the scanning rate, m stands for the mass of electroactive sample, ΔV stands for the voltage window and integral represents the CV curve area.

From the GCD curves, for the asymmetric setup, the specific capacitances can be determined using the following equation:

$$C_s = \frac{I\Delta t}{m\Delta V} \, (\mathrm{F \, g^{-1}})$$

where Δt stands for the discharging time, ΔV stands for the voltage window, and I/m stands for the current density.[48]

2. Development of MoSe$_2$ nanostructures for supercapacitor applications

2.1 Liquid-phase exfoliation method

Liquid-phase exfoliation is a solution-processing method used to produce two-dimensional nanosheets from layered materials such as graphite in large quantities. This technique involves dispersing layered crystals in a suitable solvent and applying energy to separate the layers into individual nanosheets. The most common energy sources include ultrasonication, high shear mixing, and micro fluidization, which help overcome the van der Waals forces holding the layers together. The exfoliation of MoSe$_2$ into single-layer or few-layer structures using this technique is made easier by the weak van der Waals forces between MoSe$_2$ layers in bulk MoSe$_2$, which are comparable to those between the MoS$_2$ layers in bulk MoS$_2$.[24,49] Jiang *et al.* employed a liquid-phase exfoliation technique to produce 2H MoSe$_2$ nanosheets using a precursor of MoSe$_2$ powder and a mixed solvent of water and ethanol.[50] Bath sonicator was used

for the exfoliation process, and a centrifuge was used to separate unexfoliated powders. The obtained products were further processed to prepare a thin film and an electrode to investigate their performance in SCs. In one of the reports, Rahul and Arora used the same method to produce $MoSe_2$ nanosheets using bulk $MoSe_2$ powder and isopropyl alcohol (IPA) as solvents. Sonication was done for 5 h at room temperature. The authors used a temperature-controlled water bath during the sonication process. The formation of exfoliated $MoSe_2$ nanosheets was validated by peaks in the Raman measurements. According to the FESEM result, the sample is made up of both large and small flakes and sheets that are evenly dispersed throughout the substrate surface. The structure displayed distinct crystal lattice fringes of around 0.64 nm, which were attributed to d-spacing for the (002) basal plane of $2H\text{-}MoSe_2$, according to the TEM results. The electrode made from the obtained nanosheets was further investigated by the authors for further electrochemical analyses.[51] In another study, Mendoza-Sánchez et al. reported $MoSe_2$ nanoplatelet preparation using the same method and studied their charge storage properties (Fig. 5).[52]

2.2 Microwave-assisted synthesis method

Microwave synthesis is an innovative method that utilizes microwave radiation to accelerate chemical reactions,

significantly enhancing the efficiency and speed of various synthesis processes. This technique allows for rapid heating of reaction mixtures, often reaching temperatures above the boiling point of solvents, which can lead to improved reaction kinetics and higher yields compared to conventional heating methods. Leaf-like $MoSe_2$ with mesoporous structures was synthesized by Vattikuti and co-workers using a microwave irradiation technique. A solution containing a known amount of sodium molybdate, Se powder, and PVP as surfactant was vigorously stirred for 1 h in DI water and hydrazine hydrate. Then, the solution was exposed to microwave irradiation at 160 °C for 25 min, and then finally, the precipitates were collected for further studies. The Raman and XRD images confirmed the formation of $MoSe_2$. The authors reported that the as-prepared $MoSe_2$ had a surface area of 64.63 m^2 g^{-1} and mesopore sizes of 8 nm. Mesoporous $MoSe_2$ nanostructures that resemble dry leaves are formed, as shown in SEM and HRTEM images. For 5000 cycles, the mesoporous $MoSe_2$ electrode demonstrated exceptional cycling stability while achieving a capacitance of 257.38 F g^{-1} at 1 A g^{-1}.[53]

2.3 Sonochemical method

The sonochemical method basically involves exfoliating the precursor material by applying high-intensity ultrasound energy

Fig. 5 Frequently used methods for MoSe2 synthesis. Created in BioRender. FRANCIS, M. (2024) Colloidal icon: https://BioRender.com/r76t891, Microwave icon: https://BioRender.com/o73b224, Sonochemical icon: https://BioRender.com/t91j774, Hydrothermal icon: https://BioRender.com/j53g540.

for a certain period. The solvents used, sonication power and sonication time play crucial roles in obtaining a necessary number of layers. Fig. 11 shows the schematic of a typical sonochemical synthesis route. Using H_2O_2 as an intercalating agent in isopropyl alcohol, Kirubasankar and colleagues developed a simple and efficient sonochemical method for fabricating a few layers of $MoSe_2$ nanosheets. The optimization of the synthesis process was done by testing the probe-sonicator under ice-cold conditions for three distinct periods (15, 30, and 45 minutes) at a constant power.[54] The suspensions of $MoSe_2$ were collected after centrifugation and dried to obtain final products. The authors reported that the sonication time played a crucial role in determining the number of layers and yield of the products. A distinct hexagonal phase (2H-$MoSe_2$) with a space group (P_{63}/mmc) was confirmed from the XRD patterns, and the absence of any impurity peaks suggests that a pure hexagonal phase has formed. For the exfoliated $MoSe_2$, the surface areas were determined to be 68 m^2 g^{-1}. Further other characterizations were also carried out to confirm the desired material formation. The authors examined the synthesized nanosheets for further electrode performance analysis.

2.4 Electrodeposition method

Electrodeposition, also known as electroplating or electrochemical deposition, is a process used to deposit a layer of materials, typically metal, onto a substrate through the reduction of cations from an electrolyte solution. This technique involves immersing the substrate (acting as the cathode) in an electrolyte containing metal salts. When a current is applied, metal ions migrate to the cathode, where they gain electrons and are reduced to form a solid metal layer.

A simple electrochemical deposition (ECD) method was used by Mariappan et al. to create a binder-free electrode made of $MoSe_2$ nanosheets directly grown on a Ni foam. Ammonium molybdate and selenium dioxide were added to DI water to make the growth solution. In this work, the ECD process was carried out in a three-electrode configuration with Ag/AgCl as the reference electrode, a Pt sheet as the counter electrode, and a Ni foam as the working electrode. With varying deposition times, the procedure was carried out using an applied voltage of −1.1 V (against Ag/AgCl).[55] More $MoSe_2$ nanosheets that were arbitrarily oriented and aligned on the surface of Ni foam grew as the deposition time increased. Raman characterization was done to examine the vibration bands for the prepared nanosheets. The authors concluded that the vibration bands seen in the $MoSe_2$ nanosheets generated using ECD were in good agreement with those found in earlier $MoSe_2$ research. The nanosheets were further examined in electrochemical tests for supercapacitor performance analysis.

2.5 Colloidal method

The colloidal technique involves the formation of nanoparticles through a solution-based process, where precursor materials undergo nucleation and growth in a colloidal medium. The process typically follows the classical nucleation and growth model, where the rapid formation of nuclei occurs, followed by their growth into larger particles. Colloidal synthesis helps for precise control over particle size, shape, and composition by manipulating various parameters such as precursor concentration, temperature, and the use of stabilizing ligands. Colloidal routes to $MoSe_2$ need suitable reactive precursors to accommodate the highly anisotropic crystal growth. This method has been instrumental in producing various nanomaterials including metals and semiconductors, which find applications in energy storage, catalysis, electronics, medical diagnostics, and photovoltaics. Substrate-free $MoSe_2$ nanostructures with a consistent flower-like shape and tuneable average diameters ranging from roughly 50 to 250 nm were synthesized colloidally by Sun and coworkers. Precursors included 1-octylamine, oleic acid, and sodium molybdate. For the nanoflowers, a number of highly crystalline few-layer nanosheets protruded from the central core. The authors showed that by varying the reaction time, the nanoflower sizes could be adjusted. Using XRD and TEM, the authors highlighted the formation of nanoflowers contained with nanosheets. The average crystallite size by Scherrer analysis (10 nm) was found to be smaller than that observed by TEM (50–150 nm), due to which the authors emphasized that the nanosheets are laterally polycrystalline. The distinctive first-order A_{1g}-like, and E_{2g}-like Raman active modes are detected at around 241 and 285 cm^{-1}, respectively, based on the Raman analysis. The authors confirmed that these are in perfect agreement with previous Raman experiments in $MoSe_2$.[56] Guo et al. utilized colloidal synthesis to produce $MoSe_2$ nanonetworks and nanoflowers such as morphologies. $Mo(CO)_6$, selenium (Se), 1-octadecene (ODE), oleylamine (OAm) and oleic acid (OA) were used as reactants. The authors emphasized that the ratio of OAm to OA determines the shape of $MoSe_2$ nanostructures. When OAm is not present, the synthesized products are nano-networks made up of ultrathin nanosheets that are continuously coupled in a comparatively flat pattern. The $MoSe_2$ ultrathin nanosheets tend to create random configurations in various directions as the amount of OA in the reaction increases. They can also form porous nanonetworks or discrete nanoflowers. Such morphology tuning can be further investigated for developing better surface for electrodes.[57] Wang et al. synthesized high-quality $MoSe_2$ nanospheres from the same route.[58] The microstructure consisted of uniform nanosphere agglomerates in the range of 200 to 450 nm. BET surface areas for the nanospheres were recorded to be 62.3 m^2 g^{-1}. This can be beneficial for developing high-surface area electrodes for SCs.

2.6 Hydrothermal/solvothermal method

The hydrothermal process refers to a chemical synthesis technique that employs aqueous solutions or organic-based solvents. In the hydrothermal/solvothermal process, a prepared and agitated solution is poured into an autoclave and heated in a high-pressure reactor for a predetermined amount of time at a set temperature. The desired sample is eventually produced by this process, which takes place in a high-temperature sealed enclosure within the hydrothermal/solvent system.[59] This approach provides cost-effectiveness,
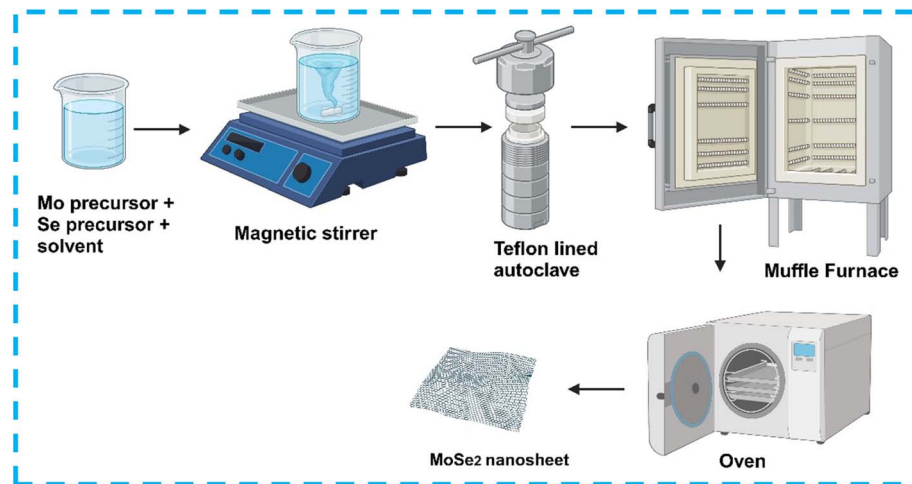
Fig. 6   Hydrothermal/solvothermal synthesis setup. Created in BioRender. FRANCIS, M. (2024) https://BioRender.com/l67e934.

ease of control over response conditions, and simplicity in operation. The size and morphology of 2D materials can be efficiently controlled by varying the hydrothermal process parameters, including substrate selection, temperature, additives, and precursor choice.[60] A schematic of hydrothermal preparation is shown in Fig. 6. Balasingam and coworkers followed a hydrothermal route to prepare a few-layered $MoSe_2$ nanosheet as an electrode material for SCs.[61] The precursors used for the hydrothermal reaction were sodium molybdate, selenium powder (Se), and $NaBH_4$. XRD and Raman results confirmed the successful synthesis of $MoSe_2$ nanosheets. The HRTEM images and Raman spectrum confirmed the formation of few-layered nanosheets. The HR-TEM pictures showed a layered crystal structure with distinct crystal lattice fringes that measure roughly 0.62 nm, which is the usual d-spacing for the structure (002) basal plane of the hexagonal crystal structure. Notably, a large surface area for the electrochemical processes is provided by the porous nature of the $MoSe_2$ nanosheet. Using an aqueous electrolyte, the authors tested the supercapacitive performance of the prepared nanosheets in a two-electrode configuration. Using a simple hydrothermal method, Qiu et al. synthesized $MoSe_2$ nanoflakes and nanorods.[62] The desired material formation was confirmed by XRD, TEM, and SEM results. According to the authors, the mesoporous structure of the nanoflakes resulted in a large BET specific surface area of 46 m^2 g^{-1} and a high porosity of 0.06

cm^3 g^{-1}. The authors further developed a solid-state symmetrical SC device of $MoSe_2$ nanoflakes/$MoSe_2$ nanorods, showing excellent energy storage capabilities. Ultrathin 1T $MoSe_2$ nanosheets with an impressive interlayer spacing of ≈1.17 nm were prepared by Jiang et al. using a straightforward solvothermal technique.[63] The spacing reported was ≈81% wider than that of pure $MoSe_2$ (0.65 nm). Xia et al. prepared nanosheets of 1T@2H $MoSe_2$ via a two-step solvothermal process, as described in Fig. 7. The crystallinity of the samples was confirmed by various structural characterizations. This work incorporated the 1T phase with 2H $MoSe_2$ nanosheets.[64]

2.7 Chemical vapor deposition method

The CVD process produces pure and high-crystallinity solid films by depositing gaseous precursors on the substrates. The precursor reacts or decomposes on the surface of the substrate material under high-temperature and -vacuum conditions. To prepare a high-quality film having an adjustable thickness, deposition parameters such as temperature, gas flow, and pressure can be changed.[59] The precursor selection also plays a vital role in the CVD growth process. The shortcomings of this method are low yield and requirement for complex instruments.

Using Se and MoO_3 as the chemical vapor supply in a mixture of H_2 and Ar gases in a horizontal tube furnace, Shaw et al. reported the first CVD development of single- and few-layer
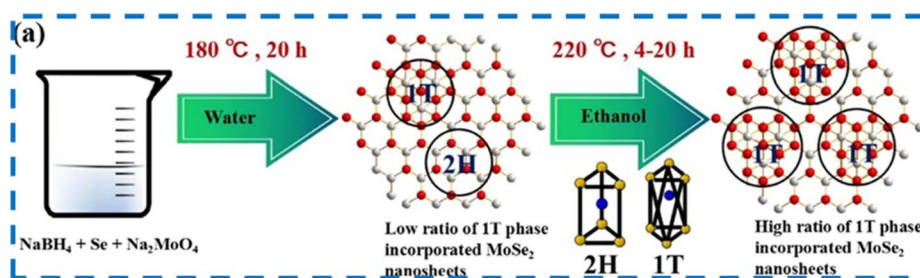

Fig. 7   Solvothermal synthesis of $MoSe_2$. This figure has been reproduced from ref. 64 with the permission from Nature, copyright 2017.

$MoSe_2$ nanosheets. It was discovered that H_2 was essential to the reaction because it promoted the reduction of MoO_3 with Se to form $MoSe_2$. The authors showed that the SiO_2/Si substrates may be used to directly generate extremely crystalline $MoSe_2$.[65] A lot of reports are available for the CVD growth of $MoSe_2$ films and nanosheets. CVD-grown $MoSe_2$ finds applications in photodetectors, flexible electronics and electrocatalysis. However, the preparation of supercapacitor electrodes from CVD-grown $MoSe_2$ has not yet been reported. This can be investigated in future to develop pure and crystalline $MoSe_2$ for energy storage applications.

2.8 Other methods

Upadhyay and Pandey successfully prepared layered $2H\text{-}MoSe_2$ nanosheets with a stacked nanoplate morphology having a hexagonal crystal structure using an *in situ* selenization process for the first time. Reaction parameters had a significant effect on the phase formation. Stacked plates with porous nanostructures were reported.[66] Various characterization results for the structural analysis of the prepared nanosheets are shown in Fig. (8–10).

3. SC performance of various $MoSe_2$ composites

3.1 Asymmetric set-up

$MoSe_2/rGO$ composites for high-performance SCs were developed employing a hydrothermal route. The effect of graphene content was studied by preparing different samples with different rGO concentrations. With the increase in rGO content, $MoSe_2$ nanospheres were uniformly dispersed on rGO

nanosheets. The composites were checked in a three-electrode setup showing optimal electrode $MoSe_2\text{-}rGO\text{-}25$, which was prepared keeping 25 mg GO initially. The rGO nanosheets helped in increasing the electrical conductivity of the sample. Moreover, by using rGO, we get contributions both from EDLC and pseudocapacitive processes. When the rGO content was increased, the diffusion of ions became slow, thereby decreasing performance.[67] Three-dimensional $CoNi_2S_4$-graphene-2D-$MoSe_2$ composites having sphere-sheet-like structures were produced by combining hydrothermal and simple ultrasonication for SC applications. Large amounts of $MoSe_2$ nanosheets and graphenes were first prepared using a liquid exfoliation technique. For comparison, various composites of $CoNi_2S_4$ such as $CoNi_2S_4$–$MoSe_2$, $CoNi_2S_4$-G, and $CoNi_2S_4$-G-$MoSe_2$ were further synthesized by the same method. The energy storage analysis revealed that the composite exhibited a maximum C_{sp} of 1141 F g^{-1} with a mass loading of 5 mg cm^{-2}. The retention of 108% was found after completion of 2000 cycles during the CV and GCD tests. Further, a symmetric device is also built showing a specific capacitance of 109 F g^{-1}.[68] Vidhya and coworkers synthesized $ZnSe@MoSe_2$ composites *via* a hydrothermal method having a flower-like morphology. The authors concluded that the flower-like structure increases electrochemical performance by offering electron mobility and additional electrolyte ions. During the CV and GCD tests, the binary electrode delivered high C_{sp} of 450 F g^{-1} at 1 A g^{-1} and retained 99.6% after completion of 2000 cycles.[69] The $Ni_{0.85}$-$Se@MoSe_2$ nanosheets were produced by the hydrothermal method on the framework of $MoSe_2$ using Nickel foam precursors. The $Ni_{0.85}Se@MoSe_2$ nanosheets exhibited C_{sp} of 774 F g^{-1}, which is twice that of $Ni_{0.85}Se$ and seven times more than
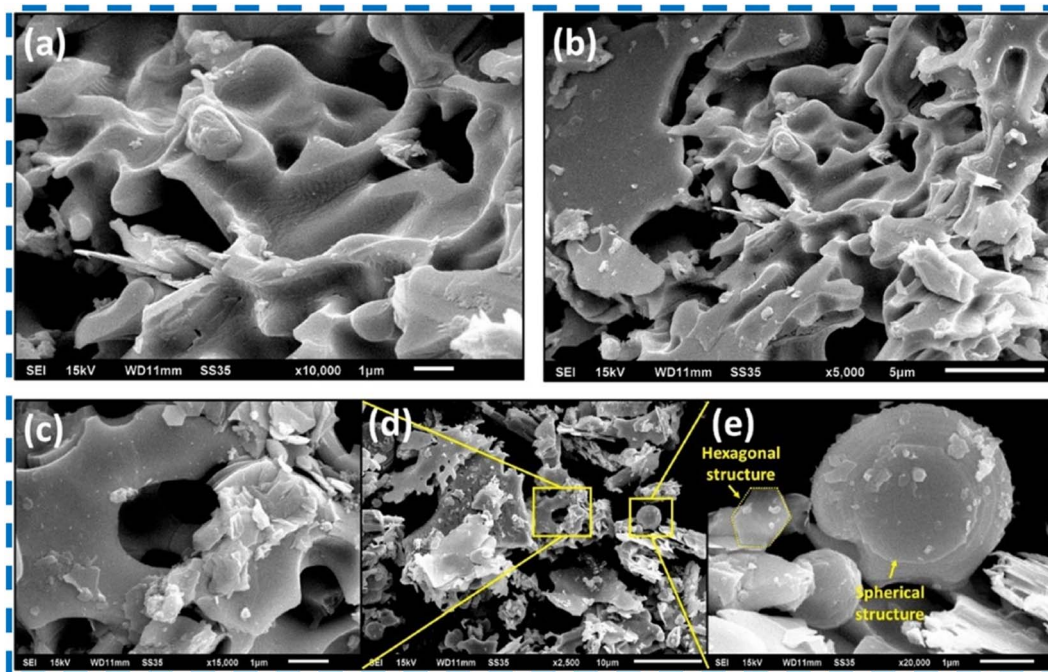

Fig. 8 (a–e) SEM results of the synthesized $MoSe_2$ powder. This figure has been reproduced from ref. 66 with permission from Elsevier, Copyright 2020.
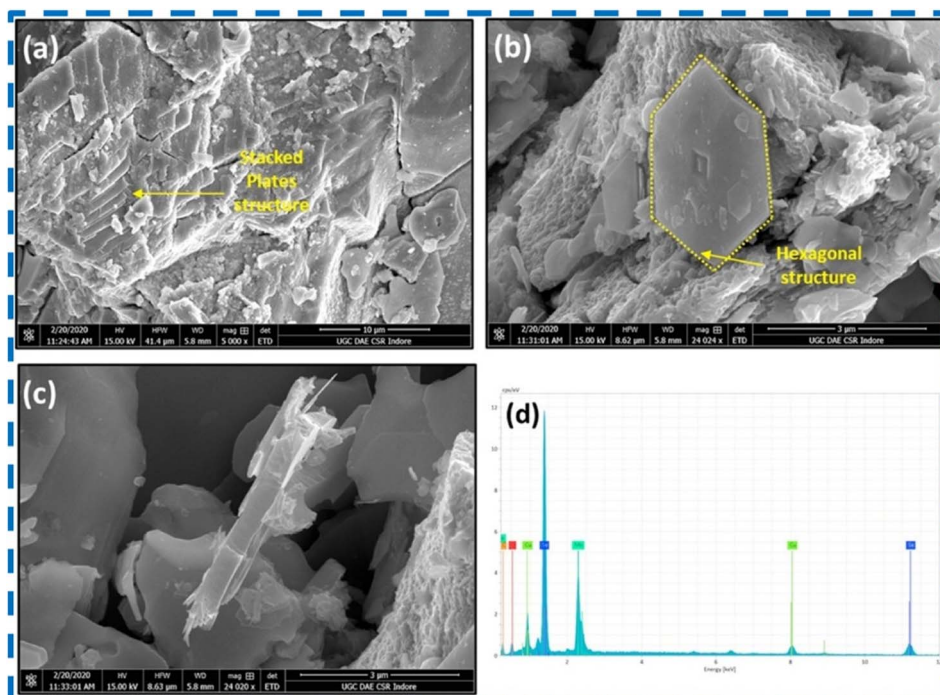
Fig. 9 (a–c) FESEM images (d) EDS of the synthesized MoSe$_2$ powder. This figure has been reproduced from ref. 66 with permission from Elsevier, Copyright 2020.

that of MoSe$_2$ nanoparticles. This was associated due to hierarchical and interconnected porous nanosheet array structures. An ASC is fabricated by the Ni$_{0.85}$Se@MoSe$_2$ nanosheet electrode, which showed an output of 1.6 V, an E_d of 25.5 W h kg^{-1} at P_d of 420 W kg^{-1}, and after completion of 5000 cycles it showed good cycling stability having 88% capacitance retention.[70] Peng and coworkers reported NiSe@MoSe$_2$ unique nanosheet arrays prepared by a hydrothermal growth method without any surfactants for high-performance ASC applications. Nickel selenide and MoSe$_2$ are similar in terms of their crystallographic structure due to the same space group. This can be useful for developing a good heterogeneous structure.[61] NiSe/MoSe$_2$/MoO$_2$ ternary composites were reported using a growth-annealing approach. The synergistic effects of MoSe$_2$, NiSe and MoO$_2$ worked well to gain good performance of the SC.[71] Gao et al. reported NiCoP nanowires decorated with few-layer MoSe$_2$ nanosheets grown on CC for the first time, employing a hydrothermal method. NiCoOH nanowires on carbon cloth were prepared via a hydrothermal reaction followed by low-temperature solid-state phosphorization to form NiCoP. A few layers with an expanded interlayer (from 0.65 nm to 0.76 nm) were seen for the composite. The composite exhibited appreciable long-term durability and at 1 mA cm^{-2} gravimetric capacitance of 5613.5 mF cm^{-2} (2245.4 F g^{-1}) was recorded. A flexible ASC was constituted using the composite as the positive electrode showing E_d of 55.1 W h kg^{-1} at P_d of 799.8 W kg^{-1}. After completion of 8000 cycles, it showed 95.8% capacitance retention revealing good cycling stability.[72] Nanosheets of layered Ti$_3$C$_2$T$_x$ MXene/MoSe$_2$ nanohybrids were hydrothermally synthesized. The authors found out that MXene flakes were enveloped inside MoSe$_2$ nanosheets. CV and GCD

measurements showed that they possess faradaic pseudocapacitive behavior. The Ti$_3$C$_2$T$_x$/MoSe$_2$ composite revealed enhanced cycling rate and specific capacitance which were better than those of MXenes and MoSe$_2$. The authors demonstrated that the observed better performance was due to expanded interlayer spacing of Ti$_3$C$_2$T$_x$ by addition of MoSe$_2$, which enhances the surface area in the electrochemical processes. High cycling ability was associated with the layered structure formation of the composite, preventing agglomeration and stacking issues. After completion of 10 000 cycles, 94.1% capacitance was retained showing good cycling resiliency.[73] Using the hydrothermal method, Guo et al. demonstrated nanoflower preparation of Na intercalated MoSe$_2$ based on mixed-phase (1T/2H) MoSe$_2$/graphene nanocomposites. The transition of MoSe$_2$ from the semiconductor to the metallic structure was observed after the addition of sodium ions. Na ion insertion causes electrolyte ions to enter the electrode, thereby enhancing the capacitance. The improved conductivity of MoSe$_2$ was due to the presence of graphene and 1T phase which enhances electrochemical activity. The authors demonstrated that the nanoflower shape, which increased the contact between electrolyte ions and the electrode, were responsible for the composite's increased electroactive area. During the CV and GCD analysis, a specific capacitance of 1407.5 F g^{-1} was recorded at 1 mV s^{-1}. An all-solid-state SC based on the prepared composite showed a specific capacitance of 244.8 F g^{-1}.[74] A hydrothermal approach was employed to develop nanohybrids of 2D MoSe$_2$/Ni(OH)$_2$, which had superb electrochemical property due to the synergistic effects. The 2D/2D hybrid displayed C_{sp} of 1175 F g^{-1}, which was better than Ni (OH)$_2$ (933 F g^{-1}) maintaining 85.6% rate capability. The nanohybrid-based
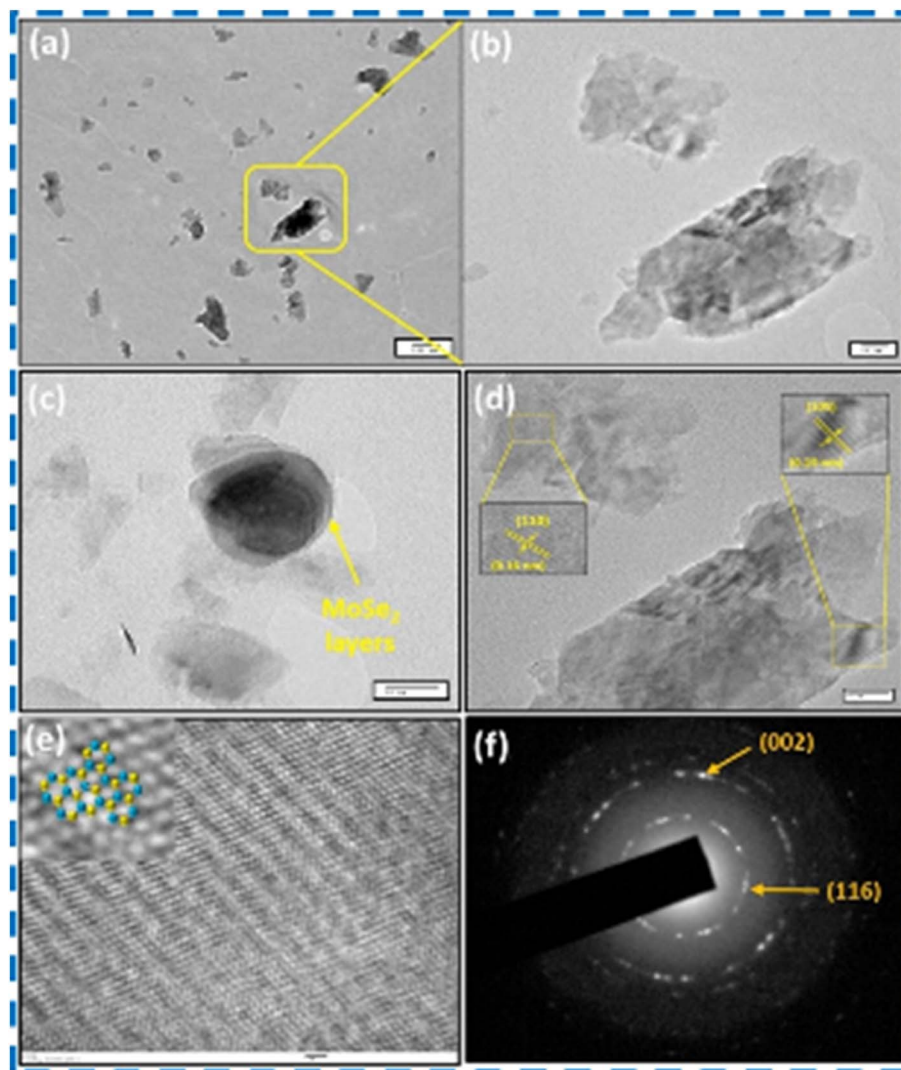
Fig. 10 (a–c) Result of TEM scan, (d) HR-TEM measurements, (e) TEM results (plan view) (f) SEAD measurements of $MoSe_2$ powder. This figure has been reproduced from ref. 66 with permission from Elsevier, Copyright 2020.

ASC recorded a high E_d value of 43 W h kg^{-1} and a high P_d value of 8181 W kg^{-1}. Even after the completion of 5000 cycles, 85% of capacitance was retained showing appreciable resiliency. It was used to light small LEDs for few minutes.[75] Karade and coworkers demonstrated the synthesis of $MoSe_2$/MWCNT(MSMC) hybrids employing a combination of dip and dry along with chemical bath deposition. The authors in this work compared the energy storage performances between $MoSe_2$, MWCNTs and MSMC using a 1 M KOH electrolyte.[76] Yu et al. reported $Ni_{0.85}Se/N–MoSe_2$ hybrids for asymmetric supercapacitors via a hydrothermal route, using water and formamide as a mixed solvent. The hybrid had a better specific capacity than that of the individual units, which was due to the cooperative effect and mesoporous structure. The electrochemical performance of the hybrid demonstrated good cyclability, retaining 105.1% of capacitance after completion of 15 000 cycles.[77] Wei et al., for the first time, successfully designed 3D $MoSe_2$ nanoflowers on an anisotropic carbon architecture. Most of the studies on $MoSe_2$ are focused on cathodes. Here,

they prepared composites for anodes. High pseudo capacitance was observed due to good specific surface area of 83.5 m^2 g^{-1} and high electrochemical activity of the nanoflowers. Contribution from both EDLC and pseudocapacitance is observed, which produces synergistic effects and helps to provide good areal capacitance.[78] A hydrothermally prepared $MoSe_2$/Ni foam showed a specific capacitance of 1114 F g^{-1} in the works of Huang and team.[79] Improvement in the specific capacitance was observed when composites are formed with carbon materials such as graphene and acetylene black. $MoSe_2$/graphene showed a specific capacitance of 1422 F g^{-1} and $MoSe_2$/acetylene black showed 2020 F g^{-1}.[80,81] A self-charging power cell was fabricated making use of $MoSe_2$ electrodes. The reported better performance was due to the use of ionogel electrolytes and intercalative-type $MoSe_2$ energy storing electrodes. The cell exhibited 18.93 mF cm^{-2} specific capacitance, 37.90 mJ cm^{-2} energy density and 268.91 μW cm^{-2} power density.[82] Arulkumar et al. reported $Ti_3C_2T_x$ MXene/$MoSe_2$ nanocomposites for ASC prepared via a hydrothermal approach. A bare Ni foam has little
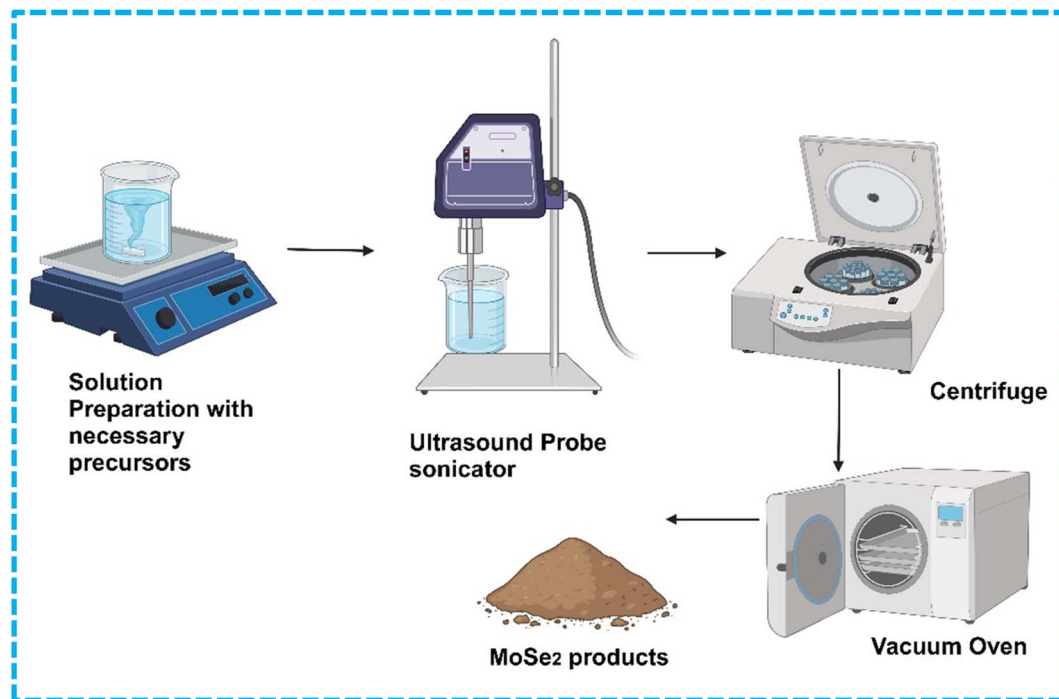
Fig. 11 Sonochemical method for $MoSe_2$ preparation. Created in BioRender. FRANCIS, M. (2024) https://BioRender.com/c76w095.

capacitance, as indicated by a flat line on the CV graph. The composite has better capacity than that of individual elements, which can be inferred from the larger area coverage in the CV plots. The diffusion control contribution slowly declines and pseudocapacitive contribution slowly increases with the increase in scan speeds. The GCD plots are non-linear and symmetrical in nature supporting the redox peaks shown in the CV plots, thereby confirming the pseudocapacitance nature. The composite exhibits the highest specific capacitance of 1531.2 F g^{-1} at 1 A g^{-1}. An ASC device was built using the composites as one of the electrodes. Good efficiency was reported which can be ascertained from the symmetric GCD profile and very negligible IR drops even when increasing current densities. The authors concluded that MXenes and $MoSe_2$ work harmoniously to produce good performance. All test results are shown in Fig. 12–14.[83]

Studies on the effect of alkaline electrolyte concentration (0.5 M, 1 M, 3 M KOH) on energy storage of $MoSe_2$/PANI were reported by Zheng and team. The samples were hydrothermally prepared using silica templates. $MoSe_2$ hollow microspheres with rough morphology were formed, which were in sizes of 740 nm contributing to the improvement in surface area. From BET analysis, it was found that the surface areas increase in the order of PANI > $MoSe_2$/PANI > $MoSe_2$. $MoSe_2$/PANI with a mass ratio of 1/1 recorded 146.5 F g^{-1} as the highest specific capacitance at 0.3 A g^{-1}. It also showed 22.16 W h kg^{-1} energy density with 198 W kg^{-1} power density. The authors concluded that good performance of $MoSe_2$/PANI was attributed to the synergistic effect of PANI and $MoSe_2$ hollow microspheres, improved conductive path, suitable electrolyte concentration, variable oxidation state, and large surface area of the material.[84] Mittal

and co-workers for the first time prepared $MoSe_2$/PANI nanocomposites and studied its electrochemical performances for supercapacitor applications. The optimized $MoSe_2$/PANI having a ratio of 1/2 showed 96% enhancement in capacitance. Testing for 3000 cycles, the composite showed capacitance retention of 72% showing good cycling stability. $MoSe_2$ performs like an EDLC material and PANI falls under a pseudo capacitance material. Forming their composite will utilize the benefits of both by synergistic effects, thereby improving the performance. Moreover, other benefits such as improved electron and ion transfer, and improved wettability of electrode were observed.[85] Zhang et al. prepared $MoSe_2$ porous nanospheres by a hydrothermal method. Nanosheets of PANI were grown in situ, and thereafter, $MoSe_2$/PANI capsule nanospheres (CNs) were synthesized. The authors noted that the composite's performance was dependent on the quantity of PANI. The best composition was found to be $MoSe_2$/PANI-16 CNs, which recorded a specific capacitance of 753.2 F g^{-1}. It was found that pseudocapacitance contribution dominated more than diffusion capacitance. Further the ASC device fabricated using the composites showed energy density of 20.1 W h kg^{-1} at 650 W kg^{-1} power density. Surface areas of $MoSe_2$ and $MoSe_2$/PANI CNs were noted to be 5.94 m^2 g^{-1} and 44.49 m^2 g^{-1} respectively. A seven-fold increment in specific surface area was seen due to the formation of composites. The composites had a good mesoporous structure, which can be confirmed by observing the pore size of $MoSe_2$ (21.15 nm) and $MoSe_2$/PANI (8.66 nm). The authors reported that the pore size decreased after adding PANI.[86] Sukanya et al. constructed an asymmetric supercapacitor based on the ternary heterostructure composite of YSe_2/$MoSe_2$/Ni_xB.[87] The electrode made from the prepared
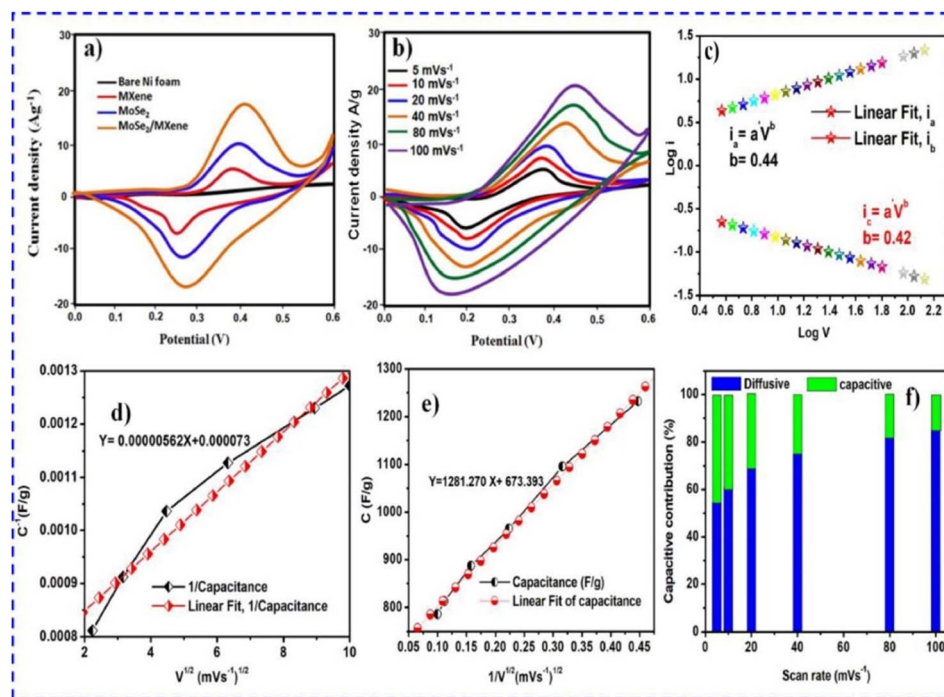
Fig. 12 (a) Cyclic voltammetry results of $Ti_3C_2T_x$ (MXene), $MoSe_2$, and composite of $MXene/MoSe_2$. (b) Cyclic voltammetry results of the composite at different scanning rates. (c) Display of the b-value of the composite. (d) Illustration of the total capacitance of the composite. (e) Capacitive contribution of the composite. (f) Diffusive and capacitive contributions of the composite. This figure has been reproduced from ref. 83 with permission from Elsevier, Copyright 2023.

Fig. 13 (a and b) Galvanostatic charging and discharging profile of $MoSe_2$ and the composite of $MXene/MoSe_2$ at 1–20 A g^{-1} (c and d) Display of stability and efficiency results for $MoSe_2$ and the composite. (e) Display of specific capacitance of $MoSe_2$ and composite at 5 mV s^{-1} to 100 mV s^{-1} (f) EIS measurements of $MoSe_2$ and the composite with the corresponding equivalent circuit. This figure has been reproduced from ref. 83 with permission from Elsevier, Copyright 2023.

Fig. 14   (a) Illustration of the assembled asymmetric device. (b) Cyclic Voltammetry (CV) results of the composite and AC. (c) Cyclic Voltammetry (CV) results of the device. (d) Display of GCD results of the device. (e) Specific capacitance *versus* current density plots for the device. (f) Stability analysis of device at 20 A g^{-1}. This figure has been reproduced from ref. 83 with permission from Elsevier, Copyright 2023.

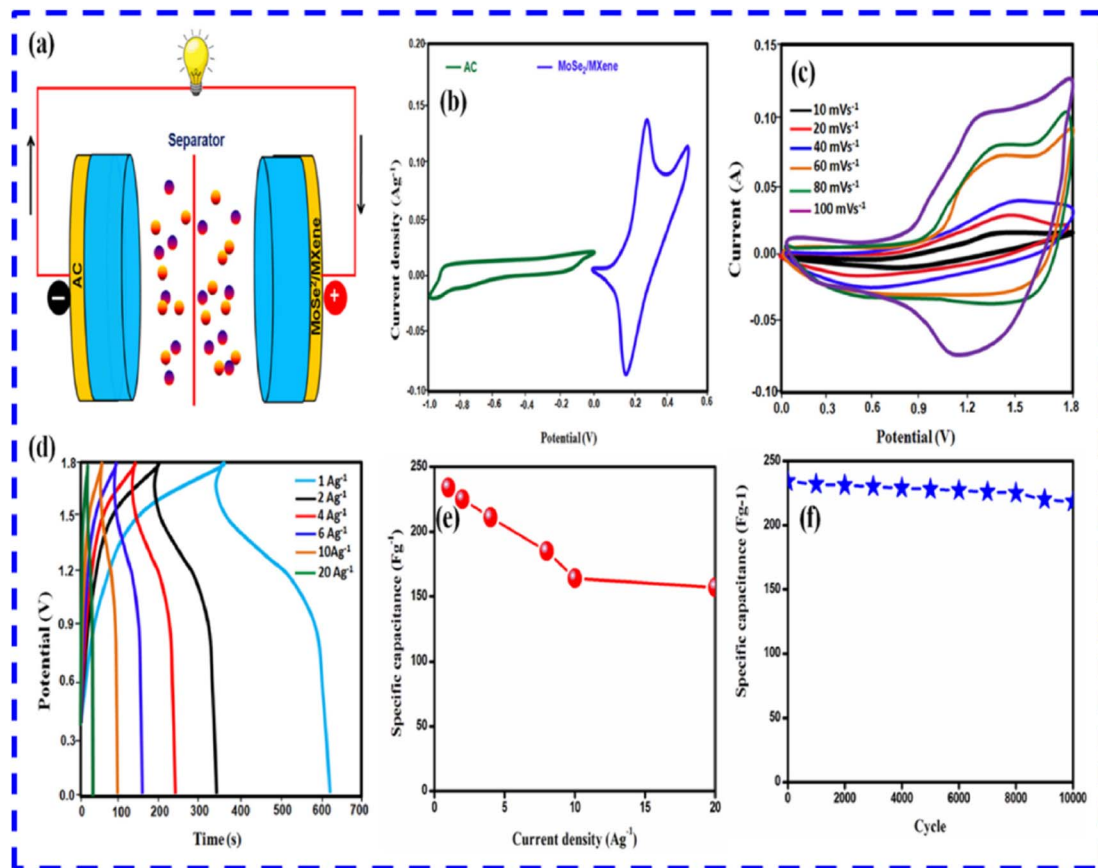composite showed 893.3 F g^{-1} as the specific capacitance and 128.17% retention after the completion of more than 5000 cycles. At 800 W kg^{-1}, the ASC device exhibited 39.5 W h kg^{-1}. Masanta and coworkers studied Mn doping on MoSe$_2$ nanostructures. Compared to pristine MoSe$_2$, 313% increment in specific capacitance was recorded when 6.2% Mn was doped.[88] Tanwar *et al.* fabricated activated carbon-coated MoSe$_2$ nanocomposites prepared *via* a hydrothermal method for high-performance aqueous supercapacitors of asymmetric type. Around 1 mg of active material was coated on the Ni foam during the tests.[89] Using a hydrothermal method, different noble metals were also explored for MoSe$_2$ composites. The authors concluded that, among them, MoSe$_2$–Au showed the highest specific capacitance. It was 1.5 times larger in comparison to bare MoSe$_2$ nanosheets.[90] Du *et al.* employing a hydrothermal method prepared nanoflowered porous MoSe$_2$/ N-doped carbon, which was utilized as the anode material in potassium-ion capacitors.[91] Lattice plane expansion is achieved by the authors. From BET analysis, it was found that the specific surface area was 228.85 m^2 g^{-1} and the pore size was 3.91 nm. Nitrogen doping and porous carbon enhanced the structural solidity and conductivity of MoSe$_2$, accelerating the reaction kinetics and promoting the transmission of electrons. Recently, Zhu *et al.* have studied the variation of morphologies of Molybdenum selenides by controlling the Mo : Se ratio.[92] MoSe$_x$

was developed on a Ni foam by an electrodeposition process and tests were done in a three-electrode setup. SEM characterization showed that the morphologies were influenced by a Mo/Se molar ratio. The authors deduced that compared to MoSe-12, the MoSe-21 and MoSe-11 compositions had better ion storage capacity. An annealing strategy was employed to improve the overall performance. He *et al.* achieved mixed-phase 3D MoSe$_2$–NiSe/NF electrodes by controlling the hydrothermal temperature. An electroactive area of 50.84 m^2 g^{-1} with a mean pore size of 10.7 nm was found using BET analysis. 2H and (2H–1T) mixed phases were observed, which had interconnected wrinkled nanosheets. Compared to individual MoSe$_2$ and NiSe, the composite had a good 3D network structure on the surface and all the available active materials were utilized to the full extent.[93] Wang and team achieved 2H semiconducting to 1T metallic phase transition in MoSe$_2$ by tungsten doping at a high temperature.[94] Yang *et al.* investigated hetero-nanostructures of MoSe$_2$/Bi$_2$Se$_3$ for supercapacitive performances. The MoSe$_2$/Bi$_2$Se$_3$ hybrids possess enhanced electrochemical properties due to large surface areas, more redox active sites, and better electron transportation. The authors showed that the hybrids demonstrated better capacitive performances than those of individual Bi$_2$Se$_3$ and MoSe$_2$.[95] Balasingam *et al.* developed MoSe$_2$/rGO nanosheets for supercapacitor applications. The nanosheet composites were

developed *via* a hydrothermal route. During CV and GCD tests, a specific capacitance of 211 F g^{-1} was recorded, and 180% capacitance retention was noted after the completion of 10 000 cycles. The authors concluded that these results are better relative to pristine MoSe$_2$. This may be due to contributions from EDLC and pseudo capacitances. The hybrid nanostructure has excellent electrochemical performance due to more electroactive sites, better electrical conductivity, small diffusion path length and fast charge transport.[96] Vidhya *et al.* reported CuSe$_2$@MoSe$_2$ (CMS) binary composite nanorods for ASC applications, which showed an improved energy density of 113 W h kg^{-1} and showed 98.1% retention after completion of 2000 cycles.[97]

3.2 Symmetric set-up

Upadhyay and Pandey fabricated a symmetric supercapacitor (SSC) based on 2H MoSe$_2$ nanosheets using Whatman paper/KOH as a solid electrolyte. The Cyclic voltammetry tests were conducted at a scanning speed of 100 mV s^{-1}. GCD tests were conducted at 1 A g^{-1}. The authors revealed that the SSC can operate in the 0–0.6 V voltage window. Above 0.6 V, the CV curves no longer maintained rectangular shapes. The SSC had good capacitive property, which can be ascertained from the CV curves which do not show many variations when the scanning rates are slowly increased. During higher scan rates around 0.3–0.4 V redox peaks were seen in the CV curves (Fig. 15), which is an indication of pseudocapacitive nature. The GCD curves were almost symmetrical throughout the tests, indicating that SSC has high reversibility. High E_d of 184.5 mW h kg^{-1} can be achieved at P_d of 74.6 mW kg^{-1} at 0.5 A g^{-1}. Then 22.6 mW h kg^{-1} of energy density was maintained at high power density (155.6 mW kg^{-1}), which was a proof that the SSC has a good rate capability. The highest specific capacitance was found to be equal to 4.1 F g^{-1} at 0.5 A g^{-1}. High cyclability with a retention of 105% even after completing 10 000 cycles and 98% of coulombic efficiency were shown after the first cycle. Then 100% increment in efficiency was seen after 10 000 cycles. Good structural stability can be confirmed due to small increment of 0.05 Ω in the ESR after 10 000 cycles. The charge transfer resistance also got decreased by 0.8 Ω, indicating good transportation of the electrolyte ions. The authors concluded that the results support the suitability of MoSe$_2$ for supercapacitors.[66] All-solid-state symmetrical SCs based on MoSe$_2$/graphene nanocomposites had modification in the lattice structure when a small amount of W ($\approx$5%) was inserted into the composite. The characteristics of W-doped MoSe$_2$/graphene were evaluated using DFT calculations. Low K$^+$ adsorption energy and a large
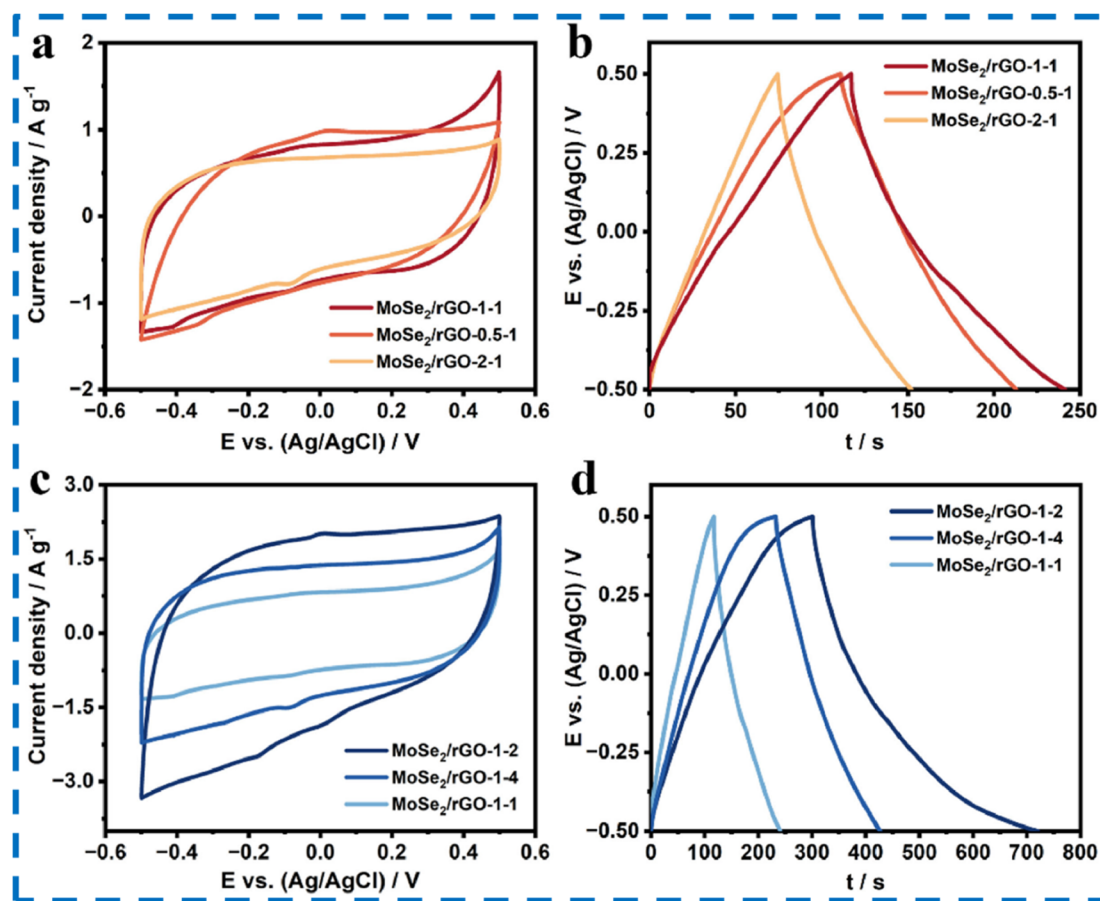

Fig. 15 (a and b) CV and GCD plots of MoSe$_2$/rGO at different concentrations of graphene oxide. (c and d) CV and GCD plots of MoSe$_2$/rGO at different Se/Mo ratios keeping the optimum graphene oxide concentration as 1 mg mL^{-1}. This figure has been reproduced from ref. 98 with permission from Elsevier, Copyright 2023.

interlayer distance were reported by the authors. The 444.4 mF cm^{-2} as specific capacity was achieved, and after 5000 cycles, 81.3% of capacitance was retained, thereby showing good stability.[99] Tanwar *et al.* reported MoSe$_2$@AC nanocomposites for SC applications *via* a hydrothermal strategy. A surface area of 522 m^2 g^{-1} with 4.6 nm mean pore size was found using BET analysis. Highest specific capacity was shown by the M@AC 1 : 5 electrode when compared with all samples. An aqueous symmetric cell using the electrode was fabricated showing 39.4 W h kg^{-1} energy density and 704.5 W kg^{-1} power density. Testing for 10 000 cycles the composite showed appreciable cyclability, and the coulombic efficiency was nearly 100%. When energy from this symmetric cell was applied for a small LED device, it could glow for around 22 min.[100] Kichi *et al.* studied electrochemical performances of layered MoSe$_2$ and selenium-rich MoSe$_2$ by the optimization of reaction parameters such as molar ratio of precursors, temperature and duration of reaction. The supercapacitor based on the MoSe$_2$ electrodes recorded C_{sp} of 122.66 F g^{-1}. The Se-rich MoSe$_2$-based supercapacitor recorded C_{sp} as 19 F g^{-1}, which was less than the previous MoSe$_2$ sample. The authors concluded that this decrease can be due to unreacted selenium, which reduces the surface area.[101] Tanwar and coworkers investigated electrochemical performances of different shaped transition metal selenides. They prepared nanoflowers of MoSe$_2$ *via* a hydrothermal method and found out that the nanoflower morphology showed better performance than CoSe$_2$ nanoneedles and NiSe$_2$ nanospheres. A symmetric supercapacitor was constructed using prepared MoSe$_2$, which displayed a maximum specific capacitance of 154 F g^{-1} during the energy storage tests.[102] MoSe$_2$/FeOOH composite formation between nanorods of iron oxide-hydroxide and nanoflowers of molybdenum diselenide

using a chemical blending technique *via* a hydrothermal route was reported by Tanwar and team. A symmetric cell was constructed recording a specific capacitance of 132 F g^{-1} keeping the voltage as 1 V. It shows capacitance retention of 100% after completion of 3000 cycles and after 10 000 cycles 100% efficiency was maintained. It provides 18.3 W h kg^{-1} energy density at 1174 W kg^{-1} power density. The average length of 546 nm and diameter of 80 nm was estimated for the FeOOH nanorods. The Ostwald ripening process was carried out, which influenced the rod and nanoflower morphology of the grown sample. The authors revealed that nanoflowers covering nanorods can be a suitable morphology for effective charge storage.[103] Shui *et al.* combined phase and interface engineering approaches to improve the energy storage ability of heterogeneous MoSe$_2$/rGO composites. The authors showed that the intercalation of Na$^+$ ions can cause phase conversion from 2H (hexagonal) semiconducting to 1T (octahedral) metallic. The authors studied the effect of the molar ratio (Se : Mo) and GO concentration on Na$^+$ intercalation. The authors found out that among all compositions the best was MoSe$_2$/rGO-1-2. The CV and GCD test results of MoSe$_2$/rGO-1-2 electrode are provided in Fig. 16. An ASSC (all solid-state symmetric SC) was developed based on the prepared composite. The prepared composite electrode revealed a high C_{sp} of 169.3 F g^{-1} at 0.5 A g^{-1}. The assembled ASSC device had energy density (4.88 W h kg^{-1}) and good cyclability (83.1% over 10 000 cycles). The device can also be a power source to glowing small LEDs for 70 s.[98] The various test results for the ASSC are shown in Fig. 17.

Tanwar and team studied aging impact of Se powders on morphology and electrochemical performances of MoSe$_2$ composites. Se powder is subjected to aging for several days in hydrazine hydrate as a reducing agent. The MoSe$_2$@AC

Fig. 16 (a) CV plot of the MoSe$_2$/rGO-1-2 electrode at different scanning speeds. (b) CV plots of the MoSe$_2$/rGO-1-2 electrode at different current densities. (c) Specific capacitance measurements. (d) Nyquist plots along with fitted curve. (e) Log peak current *versus* log scan rate. (f) Diffusion and capacitance contribution at different scanning speeds. This figure has been reproduced from ref. 98 with permission from Elsevier, Copyright 2023.

Fig. 17 (a) Schematic of the assembled MoSe$_2$/rGO ASSC device (b) CV plots with varying potential windows (c) CV plots at different scanning speeds. (d) GCD plots at different current densities. (e) Specific capacitance evaluated from GCD (f) few serially connected ASSC devices to glow a small LED. This figure has been reproduced from ref. 98 with permission from Elsevier, Copyright 2023.

Fig. 18 (a) CV plot of the MoSe$_2$/CRF composite at different scan speeds, (b) CV plot of MoSe$_2$ and the composite at 30 mV s^{-1}, (c) GCD curves of the composite at different current densities, (d) discharging profiles for MoSe$_2$ and the composite electrode at 1 A g^{-1}. This figure has been reproduced from ref. 105 with permission from Elsevier, Copyright 2021.

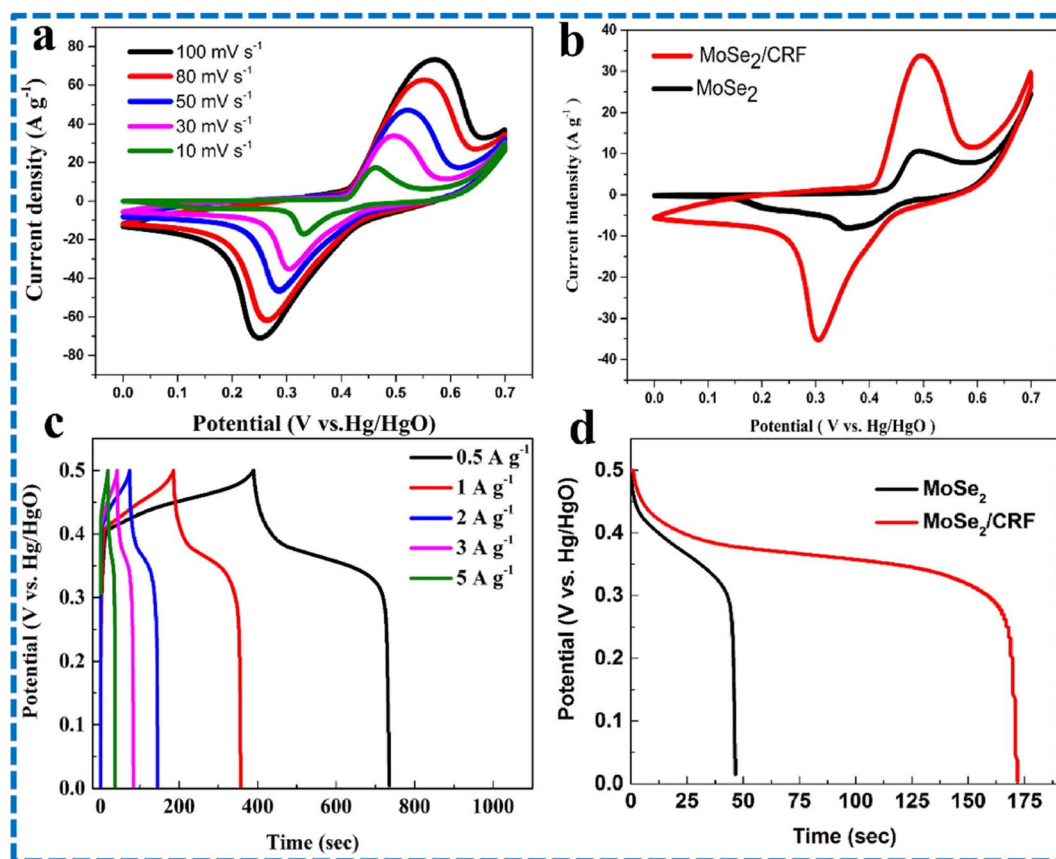composite was prepared *via* a hydrothermal route. Compared to the remaining samples, the six days aged sample showed superior performance. With the help of the fabricated symmetric cell, a few small LEDs can be illuminated.[104] The synthesis of ultrathin $MoSe_2$@carbon aerogel microspheres employing a solvent thermal method was reported by Han and coworkers. Carbon aerogels were derived from resorcinol-formaldehyde (RF) aerogels. Due to composite formation with RF, the surface area and the conductivity were increased. Various test results of the $MoSe_2$/CRF composite and $MoSe_2$ are shown in Fig. 18. CV tests were conducted at different scanning speeds employing a three-electrode system. The occurrence of faradaic reactions and the pseuodcapacitive nature of the composite were confirmed by looking into the peaks in the CV plots. The peaks become bigger on increasing the scan speeds. Compared to $MoSe_2$, the composite $MoSe_2$/CRF electrode demonstrated larger area in the CV plot, showing that it has more capacitive properties. The pseudocapacitive characteristics of the composite were further supported by the appearance of peaks in the GCD plots. The charging and discharging profiles are almost symmetric at different current densities, confirming that the redox reactions had excellent reversibility. The composite electrode outlasted the $MoSe_2$ electrode in terms of discharge time, aligning with the trends observed in the CV curves, thereby demonstrating that the composite has better specific capacitance as shown in Fig. 18. The electrode's specific

capacitance diminished as the scanning speed increased. A symmetric supercapacitor is also developed using the composites and its performances are checked. Different test results for symmetric SCs based on $MoSe_2$/CRF are shown in Fig. 19. The current density peaks increased with the increase in scanning speeds revealing the good capacitive behaviour of the symmetric SC. Linear and triangular responses in GCD plots for different current densities indicate high-rate capability and superb charge transportation. After the completion of 2500 GCD cycles, the symmetric SC retained 120.8% capacitance, indicating the excellent cyclability and stability. The authors demonstrated that the primary cause of the composite's overall enhanced performance was the presence of porous CRF microspheres.[105] Various $MoSe_2$ composite electrodes which are reported until now are shown in Table 1 along with their performances (Fig. 20).

4. Machine learning for supercapacitors

Machine Learning (ML) algorithms can realize their potential in designing and optimizing electrode materials for super-capacitors. Deep learning, artificial intelligence, and data science methodologies will be able to identify the optimal electrode material specific to a particular application with

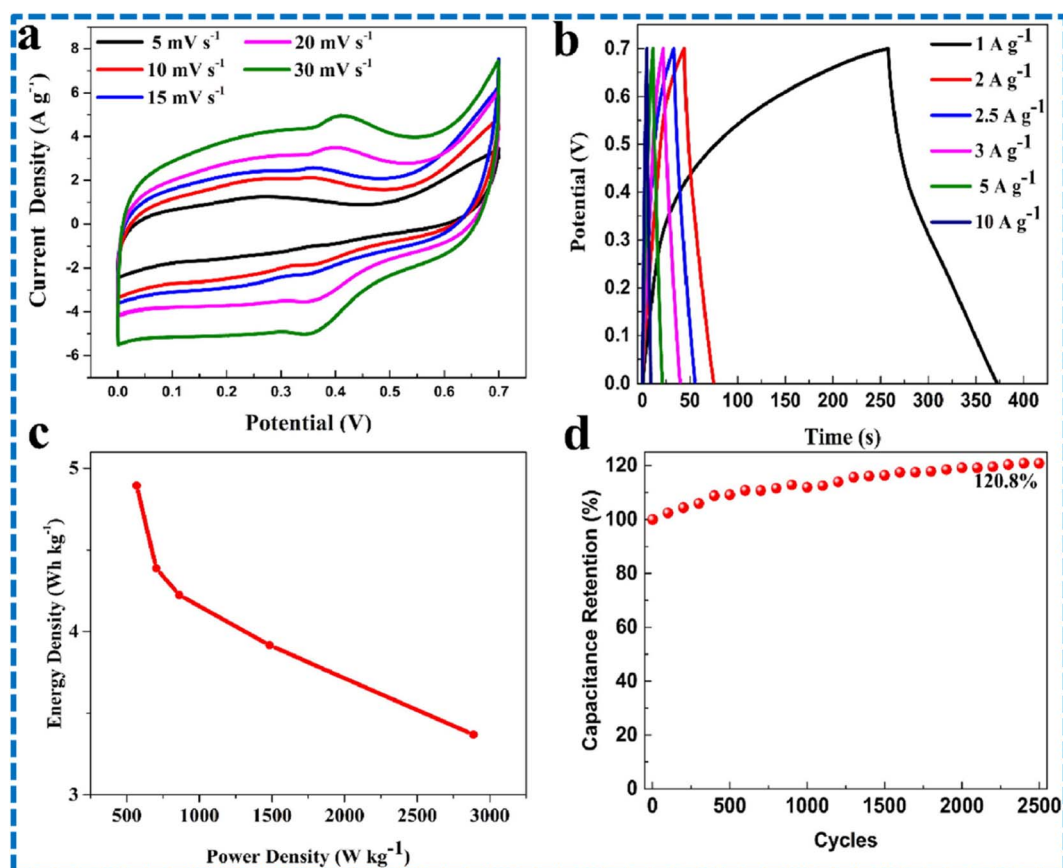Fig. 19 Symmetric SC performance of $MoSe_2$/CRF: (a) CV plots at 5–30 mV s^{-1}, (b) GCD plots at 1–10 A g^{-1}, (c) Ragone plots and (d) stability analysis. This figure has been reproduced from ref. 105 with permission from Elsevier, Copyright 2021.

Table 1 MoSe$_2$ composites with supercapacitor performances

Sl. no	Electrode	Synthesis	Morphology/structure	Electrolyte	Specific capacitance	Retention (%) after (cycles)	Ref.
1	MoSe$_2$	Liquid phase exfoliation	Nanosheets	3 M KCL	15 F g^{-1} at 0.1 A g^{-1}	95% (12)	51
2	2H-MoSe$_2$	In situ selenization method	MoSe$_2$ nanosheets	2 M KOH	46.22 mA h g^{-1} at 2 A g^{-1}	64% (2000)	66
3	MoSe$_2$	Microwave irradiation process	Dry leaf like mesoporous MoSe$_2$	0.5 M H$_2$SO$_4$	257.3 F g^{-1} at 1 A g^{-1}	95% (5000)	53
4	MoSe$_2$	Electrodeposition method	MoSe$_2$ sheets on Ni foam	1 M Na$_2$SO$_4$	325.92 mA h g^{-1} at 4 mA cm^{-2}	80% (1000)	55
5	MoSe$_2$	Solvothermal	Nanosheets	3 M KOH	272 F g^{-1} at 1 A g^{-1}	—	106
6	MoSe$_2$	Hydrothermal	Few-layered MoSe$_2$ nanosheets	0.5 M H$_2$SO$_4$	198.9 F g^{-1} at 2 mV s^{-1}	75% (10 000)	61
7	MoSe$_2$	Solid reaction, in situ selenization	Nanoflakes	1 M NaOH	25 mA h g^{-1} at 1 A g^{-1}	—	107
8	MoSe$_2$@AC symmetric cell	Hydrothermal	MoSe$_2$ nanosheets coated with activated carbon sphere	6 M KOH	394 F g^{-1} at 1 A g^{-1}	85% (3000)	104
9	MoSe$_2$@AC	Hydrothermal	Nanoflower	6 M KOH	514 F g^{-1} at 10 mV s^{-1}	68% (2500)	100
10	MoSe$_2$/C	Solvothermal	Interconnected MoSe$_2$ nanosheets and amorphous carbon	3 M KOH	878 F g^{-1} at 1 A g^{-1}	98% (2000)	108
11	Bare MoSe$_2$	Solvothermal	MoSe$_2$ nanosheets	3 M KOH	436.7 F g^{-1} at 1 A g^{-1}	72% (2000)	67
	MoSe$_2$/rGO-25	Hydrothermal	MoSe$_2$ nanosheets spheres on rGO nanosheets	2 M KOH	814.4 F g^{-1} at 1 A g^{-1}	—	
12	MoSe$_2$-rGO	Hydrothermal	MoSe$_2$ nanosheets with rGO nanosheets	0.5 M H$_2$SO$_4$	211 F g^{-1} at 5 mV s^{-1}	180% (10 000)	96
13	MoSe$_2$/rGO symmetric set-up	Hydrothermal	MoSe$_2$ nanosheets grown on rGO	2 M KOH	35.1 F g^{-1} at 0.3 A g^{-1}	83.1% (10 000)	98
14	MoSe$_2$/carbon aerogel	Solvent-thermal method	MoSe$_2$ nanosheets incorporated into carbon aerogel microspheres	1 M KOH	498 F g^{-1} at 1 A g^{-1}	127.2% (2500)	105
15	MoSe$_2$/CA	Hydrothermal	Carbon aerogel embedded in ultrathin MoSe$_2$ nanosheets	6 M KOH	775 C g^{-1} at 1 A g^{-1}	98% (1500)	109
16	Ni$_{0.85}$Se@MoSe$_2$	Hydrothermal	Ultrathin nanosheet arrays	2 M KOH	774 F g^{-1} at 1 A g^{-1}	95% (1000)	70
17	Ni$_{0.85}$Se/N-MoSe$_2$//AC	Hydrothermal	Ni$_{0.85}$Se/N-MoSe$_2$ nanosheets on N-MoSe$_2$	4 M KOH	58.4 F g^{-1} at 500 mA g^{-1}	105.1% (15 000)	77
18	NiSe$_2$@MoSe$_2$	Hydrothermal	Polyhedral structure of composite	1 M KOH	1000 F g^{-1} at 1 A g^{-1}	77.67% (5000)	110
19	NiSe@MoSe$_2$	Hydrothermal	Nanosheet arrays	2 M KOH	223 F g^{-1} at 1 A g^{-1}	93.7% (1000)	111
20	MoSe$_2$-Ni	Hydrothermal	MoSe$_2$ nanosheets on Ni foam	6 M KOH	1114 F g^{-1} at 1 A g^{-1}	104.7% (1500)	79
21	MoSe$_2$/G	Solvothermal	MoSe$_2$ nanosheets on graphene nanosheets	6 M KOH	945 F g^{-1} at 1 A g^{-1}	92% (3000)	54
22	MoSe$_2$	Sonochemical exfoliation	MoSe$_2$ nanosheets	6 M KOH	576 F g^{-1} at 1 A g^{-1}	84% (3000)	80
	MoSe$_2$-graphene/Ni	Hydrothermal	Graphene nanosheets covered on surface and interspace of MoSe$_2$ bars	6 M KOH	1422 F g^{-1} at 1.5 A g^{-1}	100.7% (1500)	
23	2H-MoSe$_2$//MoSe$_2$	Hydrothermal method	MoSe$_2$ nanosheets	0.5 M TEABF$_4$/AN	16.25 F g^{-1} at 0.75 A g^{-1}	51.26% (10 000)	112
24	MoSe$_2$/MoS$_2$	Epitaxial growth process	MoSe$_2$ thin flakes and MoS$_2$ nanosheets	0.5 M H$_2$SO$_4$	1229.6 F g^{-1} at 1 A g^{-1}	92.8% (2000)	113
25	MoSe$_2$//MoSe$_2$	Hydrothermal	Nanoflower MoSe$_2$	6 M KOH	154 F g^{-1} at 10 mV s^{-1}	16.6% (1000)	102
26	NiMoO$_4$/NiSe$_2$/MoSe$_2$	Hydrothermal method followed by selenylation	Nanowires	2 M KOH	955 F g^{-1} at 1 A g^{-1}	86.1% (5000)	114
27	NiSe/MoSe$_2$/MoO$_2$	Two-step growth annealing strategy	3D hierarchical hollow microspheres with 2D thin nanoflakes	3 M KOH	1061 F g^{-1} at 2 A g^{-1}	93.9% (10 000)	71
28	MoSe$_2$-Mo$_2$C	One-pot chemical synthesis	MoSe$_2$-Mo$_2$C hybrid nanoarrays	1 M KOH	850 F g^{-1} at 1 A g^{-1}	98% (10 000)	115
29	NiCoP@MoSe$_2$			6 M KOH	2245.4 F g^{-1} at 1 mA cm^{-2}	91.9% (8000)	72

Table 1 (*Contd.*)

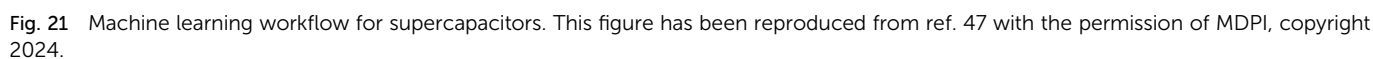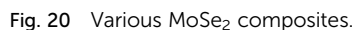| Sl. no	Electrode	Synthesis	Morphology/structure	Electrolyte	Specific capacitance	Retention (%) after (cycles)	Ref.
30	$MoSe_2/Bi_2Se_3$	Hydrothermal, phosphorization, chemical bath deposition	NiCoP nanowires on flexible CC decorated with $MoSe_2$ nanosheets	3 M KOH	1451.8 F g^{-1} at 1 A g^{-1}	—	95
31	$MoSe_2–Ni(OH)_2$	Hot injection in colloidal system	Bi_2Se_3 hexagonal nanoplates enclosed by $MoSe_2$ nanosheets	6 M KOH	1175 F g^{-1} at 1 A g^{-1}	90% (3000)	75
32	$Co(OH)_2–MoSe_2$	Hydrothermal	$MoSe_2$ nanoflakes on $Ni(OH)_2$ nanosheets	6 M KOH	541.55 F g^{-1} at 1 A g^{-1}	91.4% (3000)	116
33	$MnSe_2@MoSe_2$	Hydrothermal	Nanosheets/nanosheets	1 M KOH	719 F g^{-1} at 1 A g^{-1}	99.78% (5000)	117
34	$CuSe_2@MoSe_2$	Hydrothermal	Flowerlike morphology with nanospikes	1 M KOH	509 F g^{-1} at 1 A g^{-1}	99.82% (2000)	97
35	$MoSe_2/Ti_3C_2//MoSe_2/Ti_3C_2$	Ultrasonic reduction process	Nanorods	6 M KOH	350 F g^{-1} at 1 A g^{-1} Pure $MoSe_2$ 231 F g^{-1} Pure MXene 107 F g^{-1}	89% (5000)	118
36	$Ti_3C_2T_x/MoSe_2$	Hydrothermal	Nanosheets	6 M KOH	1358.5 F g^{-1} at 1 A g^{-1} Pure $MoSe_2$ 780.7 F g^{-1} Pure MXene 169.8 F g^{-1}	96.3% (10 000)	73
37	$Ti_3C_2T_x/MoSe_2$	Hydrothermal	$MoSe_2$ nanosheets incorporated in organ like MXene	3 M KOH	1531.2 F g^{-1} at 1 A g^{-1}	96.3% (10 000)	83
38	$MoSe_2@CN//CN$	Hydrothermal	MXene flakes with $MoSe_2$ nanosheets	1 M $LiClO_4$	101.3 mF cm^{-2} at 5 mV s^{-1}	—	119
39	$3D-CoNi_2S_4-G-MoSe2$	Liquid phase exfoliation, hydrothermal	CN decorated on $MoSe_2$ nanotubes	6 M KOH	1141 F g^{-1} at 1 A g^{-1}	108% (2000)	68
40	$FeNi_2S_4-G-MoSe_2$	*In situ* hydrothermal, liquid phase exfoliation, ultrasonication	$CoNi_2S_4$ nanoparticles on G and $MoSe_2$ nanosheets	6 M KOH	1700 F g^{-1} at 2 A g^{-1}	106% (4000)	120
41	Na ion intercalated 1T–2H $MoSe_2$-G	Hydrothermal	$FeNi_2S_4$ nanoparticles on G-$MoSe_2$ nanosheets	1 M PVA/KOH	143.6 mA hg^{-1} at 0.5 A g^{-1}	—	74
42	$MoSe_2$-VACNTF/NF	Chemical vapor deposition combined with solvothermal technique	Nanoflowers of $MoSe_2$-G composites	2 M KOH	435 F g^{-1} at 1 A g^{-1}	92% (5000)	121
43	$MoSe_2$-G	Hydrothermal and thermal annealing	$MoSe_2$ nanoflakes	1 M H_2SO_4	148.6 F cm^{-3} at 0.2 A cm^{-3}	—	122
44	W-$MoSe_2$/G	Hydrothermal method	$MoSe_2$ nanosheets	0.5 M H_2SO_4	248 F g^{-1} at 2 mV s^{-1}	102% (20 000)	48
45	$MoSe_2$/acetylene black	Hydrothermal	W Doped $MoSe_2$ nanoflowers grown on top of graphene sheets	6 M KOH	2020 F g^{-1} at 1 A g^{-1}	107.5% (1500)	81
46	$MoSe_2$/FeOOH	Hydrothermal	Net like $MoSe_2$/AB composites with $MoSe_2$ nanosheets	6 M KOH	132 F g^{-1} at 1 A g^{-1}	100% (3000)	103
47	$MoSe_2$/PANI	Hydrothermal	$MoSe_2$ nanoflowers on FeOOH nanorods	1 M KOH	146.5 F g^{-1} at 0.3 A g^{-1}	54.5% (1000)	84
48	$MoSe_2$/PANI//AC	Hydrothermal	$MoSe_2$ hollow microspheres and PANI rods	3 M KOH	85.7 F g^{-1} at 1 A g^{-1}	59% (1000)	86
49	$MoSe_2$/PANI	Hydrothermal, in-situ polymerization	$MoSe_2$ nanospheres on PANI nanosheets	—	463 F g^{-1} at 5 mV s^{-1}	72% (3000)	85
50	CoB//gCN/$MoSe_2$	Hydrothermal	Nanosheets and nanofibers	1 M KOH	356.4 F g^{-1} at 1 A g^{-1}	93% (10 000)	123
51	60-$MoSe_2$/(Ni, Co)Se_2	Synthetic encapsulation	$MoSe_2$ nanosheets in gCN sheets Hollow nanospherical structure	KOH	359.9 mA h g^{-1} at 1 A g^{-1}	83.7% (10 000)	124

Table 1 (Contd.)

Sl. no	Electrode	Synthesis	Morphology/structure	Electrolyte	Specific capacitance	Retention (%) after (cycles)	Ref.
52	YSe$_2$/MoSe$_2$/Ni$_x$B	Hydrothermal	Lamellar structure of MoSe$_2$ layers	3 M KOH	893.3 F g^{-1} at 1 A g^{-1}	128.17% (5000)	87
53	6.2% Mn doped MoSe$_2$	Hydrothermal	Mn doped MoSe$_2$ nanosheets	3 M KOH	1116 F g^{-1} at 5 mV s^{-1}	74%	88
54	(MoSe$_2$)AC//6KOH//AC	Hydrothermal	MoSe$_2$ nanoflowers coated with AC	6 M KOH	836 F g^{-1} at 10 mV s^{-1}	76% (3000)	89
55	MoSe$_2$-Pt MoSe$_2$-Ag MoSe$_2$-Au	Hydrothermal	MoSe$_2$ nanosheets	1 M H$_2$SO$_4$	1178 F g^{-1} at 1 A g^{-1} 1255 F g^{-1} at 1 A g^{-1} 1338 F g^{-1} at 1 A g^{-1}	93% (500) 88% (500) 95% (500)	90
56	MoSe$_2$/NC	Hydrothermal	MoSe$_2$ nanosheets into a 3D N doped porous carbon skeleton	1 M KFSI in combination with EC and DEC	415.1 mA h g^{-1} at 100 mA g^{-1}	71.3% (7000)	91
57	(2H-1T)MoSe$_2$-NiSe/NF//AC	Hydrothermal	Thin nanosheets	2 M KOH	150.9 F g^{-1} at 1 A g^{-1}	92.8% (50 000)	93
58	MoSe$_2$ NS-Ti	Hydrothermal	Nanosheets	2 M Na$_2$SO$_4$	525.5 F g^{-1} at 1 A g^{-1}	100% (1700)	125
59	W doped MoSe$_2$/graphene symmetric set-up	Hydrothermal	Nanoballs and nanoflowers	PVA–KOH	444.4 mF cm^{-2} at 1 mV s^{-1}	81.3% (5000)	99
60	MoSe$_2$/MWCNT-2	Hydrothermal	Ultrathin MoSe$_2$ nanosheets grown on MWCNTs	3 M KOH	927.25 F g^{-1} at 1 A g^{-1}	70.08% (3000)	126
61	MoSe$_2$/MWCNT	CBD	2D cryptomelane like MoSe$_2$ growth over MWCNTs	2 M KOH	232 F g^{-1} at 1.4 A g^{-1}	93% (1000)	76

improved efficiency. Very large datasets are used in ML-based methods, often generated through prolonged experimental research or existing literature, which train models for predicting quantities such as specific capacitance, efficiency, cyclic stability, charge–discharge times, and capacity retention.[127–131] It typically involves aggregating a plentiful amount of research data and then feeding it into sophisticated algorithms that analyze the information to generate insights relevant to the research objectives. Then, these ML models are used for projecting the performance of electrode materials and estimating parameters such as capacitance, remaining useful life, lifetime, and state of health. Moreover, ML tools allow for investigating complex correlations and interdependencies of various factors influencing electrode properties, facilitating an enhanced understanding of material behavior under different conditions.[132–142] ML applied in this context fundamentally quickens the identification of optimal electrode compositions, reducing thermal energy storage time and resources usually spent on experimental trial and error. Synthesis conditions also include the selection of an electrolyte and voltage window specifications that can, additionally, be fed into the machine learning software.[143–149] Machine learning workflow diagram for supercapacitors is shown in Fig. 21.

If blueprinting performance and accurately predicting enhancement strategies of MoSe$_2$ nanostructures for supercapacitor applications are feasible, machine learning algorithms provide an extraordinarily robust toolset for doing so. Not only algorithms like multiclass classifiers or random forest but also support vector machines contained in a class may classify nanostructures by either morphology or electrochemical properties. Following the modeling of synthesis parameters and performance metrics, regression techniques are then applied for means such as linear and support vector regression to understand how changes in production can lead to better results. Long-term stability in MoSe$_2$ electrodes was predicted with time series models such as RNNs and LSTM networks. Deep learning methods within multi-layer perceptron and deep belief networks will allow uncovering complex nonlinear dependencies between variables. Techniques like random subspace and random committee further increase predictive accuracy and robustness, thereby rendering these algorithms indispensable in stepping up research and development in supercapacitor technologies. Many research articles have used machine learning approaches that predict the capacitance of materials. The remaining useful life of SCs were predicted with the aid of machine learning techniques.[150–154] Some hybrid machine learning models have also been formulated by integrating two or more different algorithms to enhance accurate prediction; it becomes quite useful during material science and supercapacitor research. Performance assessments for these machine learning models is typically considered by different metrics as follows: Root Mean Square Error (RMSE), Mean Absolute Percentage Error (MAPE), Correlation coefficient (R^2), Mean Absolute Error (MAE), Accuracy score and error rate. These give a sense of accuracy and effectiveness of the models within their applicability domains. This

Fig. 20 Various MoSe$_2$ composites.

Fig. 21 Machine learning workflow for supercapacitors. This figure has been reproduced from ref. 47 with the permission of MDPI, copyright 2024.

ensures that the most suitable electrode materials for any supercapacitor application are found.

Using a machine learning technique, Mishra and colleagues investigated how the physicochemical features of carbon electrodes affected the performance of SCs. The ML models were trained and tested using extracted published experimental datasets having 4899 data entries to ascertain the relative significance of electrode material properties on specific capacitance. These characteristics include the carbon-based electrode material's oxygen and nitrogen content, potential window, specific surface area, pore volume and size, presence of defects and current density. Furthermore, testing procedure, electrolyte and electrode carbon structure are taken as categorical variables. Four ML techniques SVR, DT, RF, XGBoost and one Ordinary Least Square Regression (OLS) method were used to perform the regression of the target capacitance from the input

features of the SCs. MAPE, bias factor (b'), R^2, and RMSE were used as performance metrics. The best RMSE and R^2 values were displayed by the XGBoost model. The XGBoost model was reported to be best to correlate the input features with the capacitive performance. This indicates that the most important descriptors among the features chosen for the specific capacitance are potential window, specific surface area and the presence of N doping.[155] Fig. 22 shows the relationship between specific capacitance and various input features for the model. The comparison between actual capacitance and predicted capacitance for various models is shown in Fig. 23.

A study on a data-driven ML method for forecasting the capacitance of graphene-based SC electrodes was presented by Saad et al. Data from over 200 published papers has been obtained and analysed using several ML algorithms. The atomic percentages of C, N and O, I_D/I_G ratio, electrode configuration, pore-volume and size, and specific surface area were among the physicochemical characteristics used in this study. Cell configuration, potential window, ionic conductivity, current density, concentration of electrolyte, equivalent series resistance and charge-transfer resistance were among the electrochemical test characteristics derived from EIS analyses and
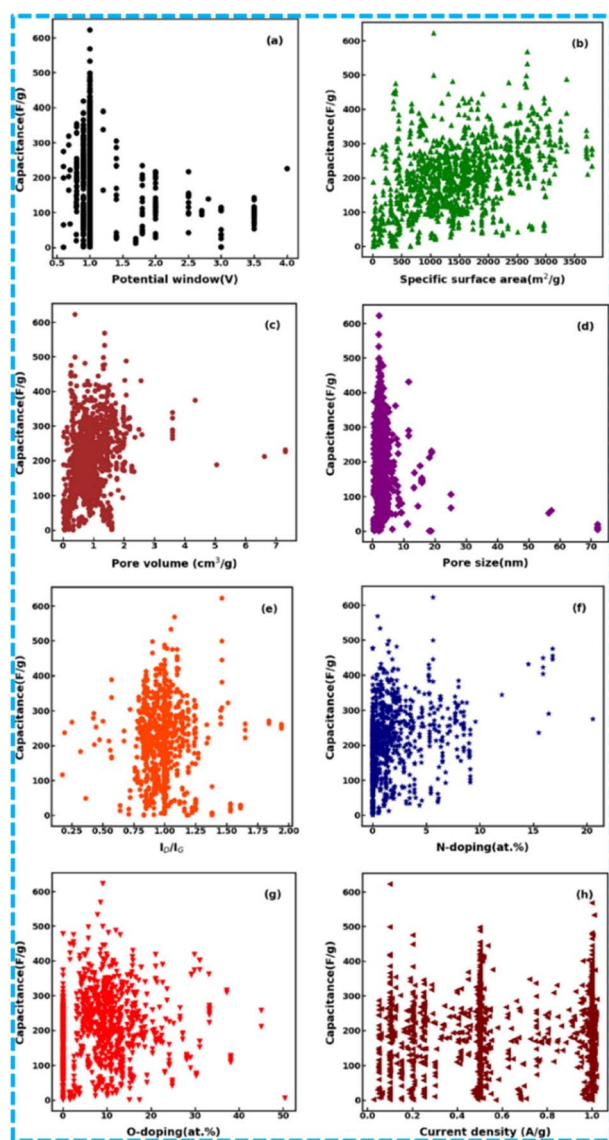

Fig. 22 (a–h) Illustration of the relationship between various input features and specific capacitance. This figure has been reproduced from ref. 155 with permission from Nature, copyright 2023.
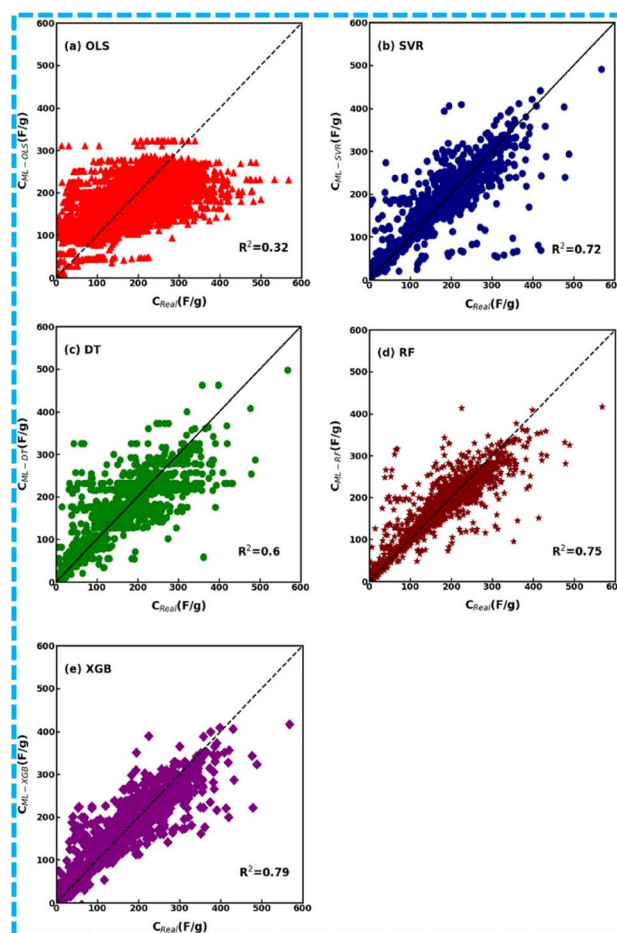

Fig. 23 (a–e) Comparison between predicted specific capacitance and actual reported specific capacitance from various models. This figure has been reproduced from ref. 155 with permission from Nature, copyright 2023.

GCD tests for the same purpose. ANN, k-nearest neighbor regression, decision trees and Bayesian ridge regression were the models used here by the authors. Comparing the constructed ANN model to other models created for this purpose, the former produced incredibly accurate prediction results, with RMSE and R^2 values of 60.42 and 0.88, respectively.[28] Deebansok and team performed analysis of various CV and GCD images using a Convolution Neural Network (CNN) model based on image classification. The authors applied supervised ML for image classification to perform electrochemical shape analysis (over 5500 CV plots and 2900 GCD plots). Schematic illustration of the model is shown in Fig. 24. The authors developed this method to address the problem of using simple binary classification to identify which electrode type (pseudocapacitor *vs.* battery) the materials belong to. The CVs and GCDs were analyzed *via* the ML model, trained with datasets obtained from a number of scientific papers. Various CNN architectures are validated and selected based on the evaluations, by applying the theoretical CV and GCD curves. The training of model is based on the classification of the signal, such as the peak *vs.* box shape for CV, and the plateau *vs.* triangular shape for GCD. The study described here has effectively addressed the issue of interpreting signals from CVs and GCDs by utilizing machine learning to categorize materials behaviours as either battery-like or pseudocapacitor-like. Using the supervised machine learning model, the authors also examined many scientific articles that contained the keywords "pseudocapacitor" (1346 articles) or "battery" (2011 articles). This allowed them to statistically analyze the number of articles that contained the keyword that contradicted their signals. In summary, the articles were chosen at random, their pertinent GCD and CV signals were taken out, and they were then simply categorized as either battery or pseudocapacitive. The authors found that 67% of the reports that contain "pseudocapacitor" as keyword align with

their experimental findings. Nevertheless, conflicting signals were found in almost half of the publications that contained "battery" as keyword. These findings support the idea that ML could significantly outperform human-based interpretation.[156]

Wang *et al.* used an ANN model to identify oxygen-rich extremely active porous carbon electrodes for aqueous SCs with the aid of machine learning. The information gathered from several literature was used to train the ANN. Surface areas of micropores and mesopores are the structural parameters employed in ANN, whereas the overall percentage of N and O doping is employed as a chemical feature. The SC performance of N/O co-doped activated carbon-based electrodes is gathered in the training database for both 6 M KOH and 1 M H_2SO_4 electrolytes. The electrolyte type is handled as a dummy variable in the ANN model. There are 288 data points in the dataset. Training, validation, and test datasets make up 70%, 15%, and 15% of the total, respectively. According to ANN's prediction, the highest capacitance of a N/O co-doped activated carbon electrode in 1 M H_2SO_4 can be attained with a micropore surface area of 1502 $m^2\ g^{-1}$, a mesopore surface area of 687 $m^2\ g^{-1}$, nitrogen doping of 0.5 at%, and oxygen doping of 20 at%. The ANN prediction states that excessive oxygen doping in 1 M H_2SO_4 would provide a notable rise in specific capacitance because it would improve the electrode surface wetting and increase the electronic conductivity.[157] Various ML models are utilized for SC applications such as CNN, SVM, RNN, Regression models, XGBoost, Random Forests, Decision trees, and KNN. The choice of model for specific application depends on the type of data, number of datasets, and type of task (analysis, comparison, prediction, and classification). Each model has its own benefits and disadvantages. If possible, the researcher can apply the data to all models and compare their performances based on accuracy, error and other metrics. The model which shows good performance in metrics can be selected
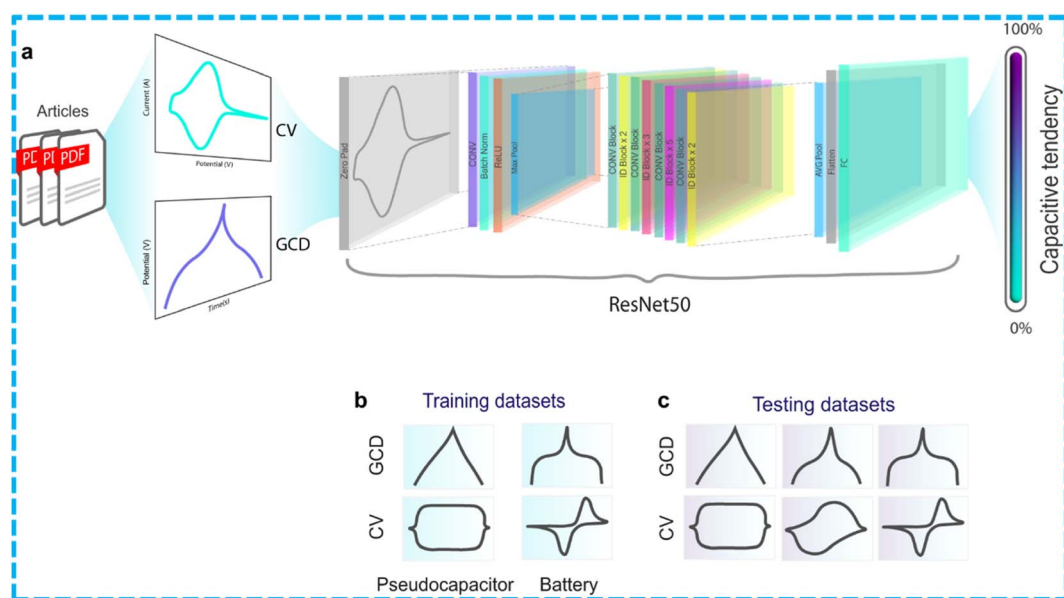

Fig. 24 (a) CV and GCD image extraction and classification from reported papers (b and c) representative of testing and training datasets. This figure has been reproduced from ref. 156 with permission from Nature, copyright 2024.

accordingly. However, this approach is suitable for small sets of data. Several researchers have selected neural network models since they can handle large and complex datasets. Other models are also beneficial depending upon the requirements of the purpose.

5. Challenges and future perspectives

(1) Using the formula $E = 0.5CV^2$, energy density was calculated for a SC electrode. From this, the energy density can be improved either by expanding the voltage window or by increasing the capacitance. The capacitance of $MoSe_2$ electrodes can be enhanced by creating highly porous structures and making composites or heterostructures with advanced capacitive materials. The voltage window can be expanded by properly selecting suitable electrolytes.

(2) Due to repeated charging/discharging and volume expansion, the $MoSe_2$ electrodes undergo structural collapse and damage. This affects their capacitance performances to a great extent. New strategies should be identified and adopted to prepare highly efficient $MoSe_2$ electrodes.

(3) The intrinsic electrical conductivity of $MoSe_2$ is very less, therefore it is not suitable for practical applications. The electrical conductivity can be improved *via* doping mechanisms, better morphology structures, adopting conductive substrates, nanosheet fabrication and composite formation with highly conductive materials.

(4) Slow ion transport hinders the overall performance of $MoSe_2$-based electrodes. This can be tackled by selecting proper electrolytes, developing microporous electrodes which can facilitate fast ion diffusion processes.

(5) Researchers have found that the 1T phase of $MoSe_2$ is metallic in nature, possessing very interesting properties. However, it suffers from structural and thermodynamic instability, and hence, not suitable for practical applications. Only few reports are available for 1T $MoSe_2$ and 1T/2H mixed $MoSe_2$-based supercapacitor electrodes. Numerous research studies need to be devoted to the development of stable 1T-phase $MoSe_2$. Phase engineering can be a modification strategy for $MoSe_2$ materials, because it can help to gain high intrinsic conductivity, promoting electron transfer and decreasing internal resistance, which are necessary for SCs. Many researchers have reported several methods to obtain phase change from 2H $MoSe_2$ to 1T $MoSe_2$ and enrich the energy storage capabilities.[24]

(6) Interfacial engineering which usually modifies the surface of $MoSe_2$ with functional materials to enhance or modify its inherent characteristics can be explored for SC applications. There are four uses for interfacial engineering: increasing catalytic performance, modifying the bandgap of $MoSe_2$, functionalizing the $MoSe_2$ interface, and promoting electron transfer. Conductive carbon materials and metal compounds are usually employed as backbones in this type of modifications. Interfacial engineering can be made to modify $MoSe_2$-based materials for the fabrication of SCs because it can create various pathways for electron transmission and distribution of $MoSe_2$ nanosheets.[24]

(7) Depending on the doped components, doping engineering can give pure $MoSe_2$ a variety of advantageous features. To create materials with the best performance, doping techniques can be employed in addition to single-heteroatom doping. To fully realize the potential of the doped heteroatoms, more research should be done to identify the ideal experimental settings for various dopants. The number of active sites can be revealed on the surface of pure materials by introducing defects and vacancies, and the disorganized configuration of active sites encourages reactant adsorption and activation. One effective method for improving the poor conductivity of $MoSe_2$ is vacancy engineering, and the degree of improvement is directly correlated with the quantity of Se vacancies. Thus, additional research ought to be carried out to investigate the possibilities of vacancy engineering and broaden its uses.[24]

(8) Inherent drawbacks of $MoSe_2$ in SC applications can be mitigated by structural engineering, which can change their physical characteristics. The structural changes employed to customize the redox activity and speed up electron transmission in the $MoSe_2$ interlayers are anticipated to have considerable practicality and application potentials since $MoSe_2$ has a layered structure with a wide interlayer spacing. This can be an effective method for expanding active sites and speeding up electron transport.[24]

(9) Recently, a new 2D material borophene has shown good promise to be used in energy storage devices. Still now, no reports are available on $MoSe_2$/borophene composites. This can be done in future to examine their energy storage abilities for supercapacitor applications.

(10) Integrating $MoSe_2$ SCs with other devices such as sodium-ion batteries and lithium-ion batteries and other types of batteries can leverage the advantages of both batteries and
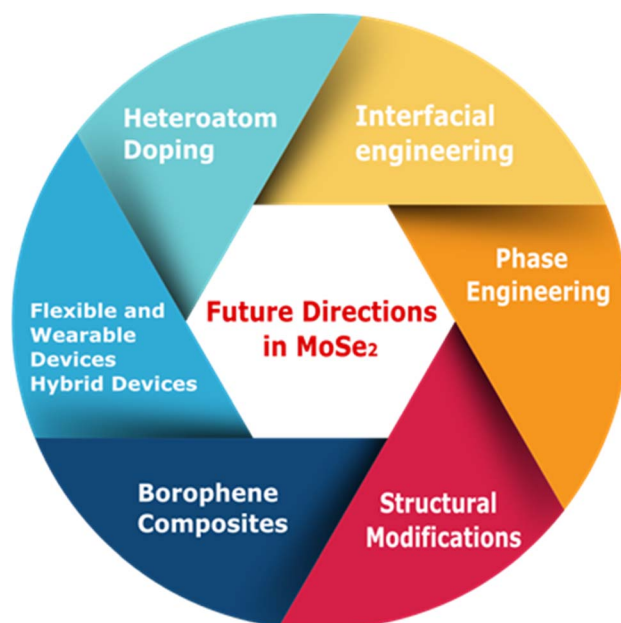

Fig. 25 Future Directions for $MoSe_2$ Supercapacitors.

supercapacitors, offering high energy densities and power densities.

(11) $MoSe_2$ SCs can find applications in various flexible and wearable devices, which are in high demand in the future, provided that sufficient research attention is paid in this field. These devices require very flexible small efficient nano electrodes for their operation. $MoSe_2$ electrodes can be developed accordingly as per requirements. This can be studied and developed in the future (Fig. 25).

6. Summary

Developing optimum electrodes is crucial for obtaining high-performance supercapacitors. Various materials are tested for electrode preparations. $MoSe_2$-based electrodes attract considerable attention in 2D materials and in the area of supercapacitor applications. $MoSe_2$ can be a good substitute for MoS_2 and other 2D electrodes. $MoSe_2$ stands as a good pseudocapacitive material. In this review, we discussed various synthesis approaches utilized for $MoSe_2$ preparation for supercapacitor applications. Most researchers have used hydrothermal methods frequently. Various structures and morphologies are reported using different synthesis and operating conditions. Each method has its own benefits and shortcomings. A brief discussion about supercapacitor fundamentals was mentioned along with working and classifications. The performance of various $MoSe_2$ composites was analyzed for asymmetric and symmetric supercapacitors along with a comparison table. Further, machine learning methods for supercapacitors are briefly described for capacitance predictions, remaining useful life predictions, life-time calculations and forecasting useful details, emphasizing that the use of ML is inevitable in the coming days in the area of energy storage. Current challenges and prospects are also provided at the end.

Data availability

No primary research results, software or code have been included and no new data were generated or analyzed as part of this review.

Conflicts of interest

There are no conflicts to declare.

Acknowledgements

References

1 A. Anastasovski, M. B. Andreucci, J. Kadar and M. Delli Paoli, Energy Storage in Urban Areas: The Role of Energy Storage Facilities-a Review, *Energies*, 2024, **17**, 1117.

2 R. Kumar, D. Lee, U. Agbulut, S. Kumar, S. Thapa, A. Thakur, R. D. Jilte, C. A. Saleel and S. Shaik, Different energy storage techniques: recent advancements, applications, limitations, and efficient utilization of sustainable energy, *J. Therm. Anal. Calorim.*, 2024, **149**, 1895–1933.

3 C. Forsberg, Addressing the low-carbon million-gigawatt-hour energy storage challenge, *Electr. J.*, 2021, **34**, 107042.

4 A. M. Nasture, M. S. Raboaca, L. Patularu and C. Lupu, in *Energy Storage Systems: from Classic to Hydrogen*, IGI Global, 2021, pp. 105–138.

5 P. Duffy, C. Fitzpatrick, T. Conway, and R. P. Lynch, in *Energy Storage Options and Their Environmental Impact*, ed. R. E. Hester and R. M. Harrison, The Royal Society of Chemistry, 2018, pp. 1–41.

6 B. K. Kim, S. Sy, A. Yu and J. Zhang, Electrochemical Supercapacitors for Energy Storage and Conversion, in *Handbook of Clean Energy Systems*, Wiley, 2015, pp. 1–25.

7 C. Portet, P. L. Taberna, P. Simon, E. Flahaut and C. Laberty-Robert, High power density electrodes for Carbon supercapacitor applications, *Electrochim. Acta*, 2005, **50**, 4174–4181.

8 J. Zhang, G. Zhang, T. Zhou and S. Sun, Recent Developments of Planar Micro-Supercapacitors: Fabrication, Properties, and Applications, *Adv. Funct. Mater.*, 2020, **30**, 1910000.

9 T. Ramachandran, S. S. Sana, K. D. Kumar, Y. A. Kumar, H. H. Hegazy and S. C. Kim, Asymmetric supercapacitors: Unlocking the energy storage revolution, *J. Energy Storage*, 2023, **73**, 109096.

10 C. Zhao, Y. Liu, S. Beirne, J. Razal and J. Chen, Recent Development of Fabricating Flexible Micro-Supercapacitors for Wearable Devices, *Adv. Mater. Technol.*, 2018, **3**, 1800028.

11 S. Rani, N. Kumar and Y. Sharma, Recent progress and future perspectives for the development of micro-supercapacitors for portable/wearable electronics applications, *JPhys Energy*, 2021, **3**, 032017.

12 D. Gao, Z. Luo, C. Liu and S. Fan, A survey of hybrid energy devices based on supercapacitors, *Green Energy Environ.*, 2023, **8**, 972–988.

13 E. Faggioli, P. Rena, V. Danel, X. Andrieu, R. Mallant and H. Kahlen, Supercapacitors for the energy management of electric vehicles, *J. Power Sources*, 1999, **84**, 261–269.

14 J. Cherusseri, D. Pandey and J. Thomas, Symmetric, Asymmetric, and Battery-Type Supercapacitors Using Two-Dimensional Nanomaterials and Composites, *Batteries Supercaps*, 2020, **3**, 860–875.

15 K. S. Kumar, N. Choudhary, Y. Jung and J. Thomas, Recent Advances in Two-Dimensional Nanomaterials for Supercapacitor Electrode Applications, *ACS Energy Lett.*, 2018, **3**, 482–495.

16 Y. Liu and X. Peng, Recent advances of supercapacitors based on two-dimensional materials, *Appl. Mater. Today*, 2017, **7**, 1–12.

17 M. Ali, A. M. Afzal, M. W. Iqbal, S. Mumtaz, M. Imran, F. Ashraf, A. Ur Rehman and F. Muhammad, 2D-TMDs based electrode material for supercapacitor applications, *Int. J. Energy Res.*, 2022, **46**, 22336–22364.

18 N. Joseph, P. M. Shafi and A. C. Bose, Recent Advances in 2D-MoS2 and its Composite Nanostructures For Supercapacitor Electrode Application, *Energy Fuel.*, 2020, **34**, 6558–6597.

19 P. Forouzandeh and S. C. Pillai, Two-dimensional (2D) electrode materials for supercapacitors, *Mater. Today: Proc.*, 2020, **41**, 498–505.

20 J. A. Wilson and A. D. Yoffe, The transition metal dichalcogenides discussion and interpretation of the observed optical, electrical and structural properties, *Adv. Phys.*, 1969, **18**, 193–335.

21 Y. Zhao, Y. Yan and J. M. Lee, Recent progress on transition metal diselenides from formation and modification to applications, *Nanoscale*, 2022, **14**, 1075–1095.

22 M. Ali, A. M. Afzal, M. W. Iqbal, S. Mumtaz, M. Imran, F. Ashraf, A. Ur Rehman and F. Muhammad, 2D-TMDs based electrode material for supercapacitor applications, *Int. J. Energy Res.*, 2022, **46**, 22336–22364.

23 F. Davoodi and N. Granpayeh, Nonlinear manipulation of surface plasmons on graphene-TMDC Bragg reflectors, *Opt. Quantum Electron.*, 2019, **51**, 9.

24 Y. Li, M. Wang and J. Sun, Molecular Engineering Strategies toward Molybdenum Diselenide Design for Energy Storage and Conversion, *Adv. Energy Mater.*, 2022, **12**, 2202600.

25 M. Jiang, J. Zhang, M. Wu, W. Jian, H. Xue, T. W. Ng, C. S. Lee and J. Xu, Synthesis of 1T-MoSe 2 ultrathin nanosheets with an expanded interlayer spacing of 1.17 nm for efficient hydrogen evolution reaction, *J. Mater. Chem. A*, 2016, **4**, 14949–14953.

26 S. Kaur, A. Kumar, S. Srivastava and K. Tankeshwar, Electronic properties of Phosphorene/MoSe$_2$ vertical hetero-structures, *AIP Conf. Proc.*, 2017, **1832**, 050049.

27 S. Jha, M. Yen, Y. S. Salinas, E. Palmer, J. Villafuerte and H. Liang, Machine learning-assisted materials development and device management in batteries and supercapacitors: performance comparison and challenges, *J. Mater. Chem. A*, 2023, **11**, 3904–3936.

28 A. G. Saad, A. Emad-Eldeen, W. Z. Tawfik and A. G. El-Deen, Data-driven machine learning approach for predicting the capacitance of graphene-based supercapacitor electrodes, *J. Energy Storage*, 2022, **55**, 105411.

29 A. Emad-Eldeen, M. A. Azim, M. Abdelsattar and A. AbdelMoety, Utilizing machine learning and deep learning for enhanced supercapacitor performance prediction, *J. Energy Storage*, 2024, **100**, 113556.

30 M. Meuwly, Machine Learning for Chemical Reactions, *Chem. Rev.*, 2021, **121**, 10218–10239.

31 M. S. Johnson and W. H. Green, A machine learning based approach to reaction rate estimation, *React. Chem. Eng.*, 2024, **9**, 1364–1380.

32 S. Wang, K. Huang, C. Lian and H. Liu, in *Supercapacitors: Materials, Design, and Commercialization*, Elsevier, 2024, pp. 353–370.

33 C. Liu, Q. Li and K. Wang, State-of-charge estimation and remaining useful life prediction of supercapacitors, *Renew. Sustain. Energy Rev.*, 2021, **150**, 111408.

34 D. Li, S. Li, S. Zhang, J. Sun, L. Wang and K. Wang, Aging state prediction for supercapacitors based on heuristic kalman filter optimization extreme learning machine, *Energy*, 2022, **250**, 123773.

35 S. Nanda, S. Ghosh and T. Thomas, Machine learning aided cyclic stability prediction for supercapacitors, *J. Power Sources*, 2022, **546**, 231975.

36 V. Sawant, R. Deshmukh and C. Awati, Machine learning techniques for prediction of capacitance and remaining useful life of supercapacitors: A comprehensive review, *J. Energy Chem.*, 2023, **77**, 438–451.

37 N. I. Jalal, R. I. Ibrahim and M. K. Oudah, Review on Supercapacitors: types and components, *J. Phys.: Conf. Ser.*, 2021, **1973**, 012015.

38 M. V. Kiamahalleh, S. H. S. Zein, G. Najafpour, S. A. Sata and S. Buniran, Multiwalled Carbon Naotubes based nanocomposites for supercapacitors: A review on electrode materials, *Nano*, 2012, **7**, 1230002.

39 A. G. Olabi, Q. Abbas, A. A. Makky and M. A. Abdelkareem, Supercapacitors as next generation energy storage devices: Properties and applications, *Energy*, 2022, **248**, 123617.

40 H. Choi and H. Yoon, Nanostructured electrode materials for electrochemical capacitor applications, *Nanomaterials*, 2015, **5**, 906–936.

41 Z. S. Iro, C. Subramani and S. S. Dash, A brief review on electrode materials for supercapacitor, *Int. J. Electrochem. Sci.*, 2016, **11**, 10628–10643.

42 P. Simon and Y. Gogotsi, Materials for electrochemical capacitors, *Nat. Mater.*, 2008, **7**, 845–854.

43 S.-M. Chen, R. Ramachandran, V. Mani and R. Saraswathi, Recent Advancements in Electrode Materials for the High-performance Electrochemical Supercapacitors: A Review, *Int. J. Electrochem. Sci.*, 2014, **9**, 4072–4085.

44 J. Theerthagiri, K. Karuppasamy, G. Durai, A. ul H. S. Rana, P. Arunachalam, K. Sangeetha, P. Kuppusami and H. S. Kim, Recent Advances in Metal Chalcogenides (MX; X = S, Se) Nanostructures for Electrochemical Supercapacitor Applications: A Brief Review, *Nanomaterials*, 2018, **8**, 256.

45 P. Sharma and V. Kumar, Current technology of supercapacitors: A review, *J. Electron. Mater.*, 2020, **49**, 3520–3532.

46 K. V. Sankar and R. K. Selvan, The ternary MnFe2O4/graphene/polyaniline hybrid composite as negative electrode for supercapacitors, *J. Power Sources*, 2015, **275**, 399–407.

47 Q. A. Sial, U. Safder, S. Iqbal and R. B. Ali, Advancement in Supercapacitors for IoT Applications by Using Machine Learning: Current Trends and Future Technology, *Sustainability*, 2024, **16**, 1516.

48 K. S. Bhat and H. S. Nagaraja, Effect of isoelectronic tungsten doping on molybdenum selenide nanostructures and their graphene hybrids for supercapacitors, *Electrochim. Acta*, 2019, **302**, 459–471.

49 R. Sharma, A. Dawar, S. Ojha, R. Laishram, V. G. Sathe, R. Srivastava and O. P. Sinha, A Thrifty Liquid-Phase Exfoliation (LPE) of MoSe2 and WSe2 Nanosheets as

Channel Materials for FET Application, *J. Electron. Mater.*, 2023, **52**, 2819–2830.

50 Z. Jiang, Y. Wang, S. Yuan, L. Shi, N. Wang, J. Xiong, W. Lai, X. Wang, F. Kang, W. Lin, C. P. Wong and C. Yang, Ultrahigh-Working-Frequency Embedded Supercapacitors with 1T Phase MoSe$_2$ Nanosheets for System-in-Package Application, *Adv. Funct. Mater.*, 2019, **29**, 1807116.

51 Rahul and S. Kumar Arora, MoSe2 nanosheets as an efficient electrode material for supercapacitors, *Mater. Today Proc.*, 2022, **54**, 728–732.

52 B. Mendoza-Sánchez, J. Coelho, A. Pokle and V. Nicolosi, A study of the charge storage properties of a MoSe$_2$ nanoplatelets/SWCNTs electrode in a Li-ion based electrolyte, *Electrochim. Acta*, 2016, **192**, 1–7.

53 S. V. P. Vattikuti, K. C. Devarayapalli, P. C. Nagajyothi and J. Shim, Microwave synthesized dry leaf-like mesoporous MoSe$_2$ nanostructure as an efficient catalyst for enhanced hydrogen evolution and supercapacitor applications, *Microchem. J.*, 2020, **153**, 104446.

54 B. Kirubasankar, S. Vijayan and S. Angaiah, Sonochemical synthesis of a 2D-2D MoSe 2/graphene nanohybrid electrode material for asymmetric supercapacitors, *Sustain. Energy Fuels*, 2019, **3**, 467–477.

55 V. K. Mariappan, K. Krishnamoorthy, P. Pazhamalai, S. Sahoo and S. J. Kim, Electrodeposited molybdenum selenide sheets on nickel foam as a binder-free electrode for supercapacitor application, *Electrochim. Acta*, 2018, **265**, 514–522.

56 D. Sun, S. Feng, M. Terrones and R. E. Schaak, Formation and Interlayer Decoupling of Colloidal MoSe$_2$ Nanoflowers, *Chem. Mater.*, 2015, **27**, 3167–3175.

57 W. Guo, Y. Chen, L. Wang, J. Xu, D. Zeng and D. L. Peng, Colloidal synthesis of MoSe2 nanonetworks and nanoflowers with efficient electrocatalytic hydrogen-evolution activity, *Electrochim. Acta*, 2017, **231**, 69–76.

58 H. Wang, L. Wang, X. Wang, J. Quan, L. Mi, L. Yuan, G. Li, B. Zhang, H. Zhong and Y. Jiang, High quality MoSe2 nanospheres with superior electrochemical properties for sodium batteries, *J. Electrochem. Soc.*, 2016, **163**, A1627–A1632.

59 Y. Zhang, R. Zhang, Y. Guo, Y. Li and K. Li, A review on MoS2 structure, preparation, energy storage applications and challenges, *J. Alloys Compd.*, 2024, **998**, 174916.

60 H. Liu, J. Nai, F. Wang, X. Li, M. Yan, M. Qi, Y. Liu, W. Xu, G. Liu and Z. Yang, The preparation and utilization of two-dimensional materials in electrochemical energy storage, *Ionics*, 2024, DOI: 10.1007/s11581-024-05859-w.

61 S. K. Balasingam, J. S. Lee and Y. Jun, Few-layered MoSe 2 nanosheets as an advanced electrode material for supercapacitors, *Dalton Trans.*, 2015, **44**, 15491–15498.

62 Y. Qiu, X. Li, M. Bai, H. Wang, D. Xue, W. Wang and J. Cheng, Flexible full-solid-state supercapacitors based on self-assembly of mesoporous MoSe2 nanomaterials, *Inorg. Chem. Front.*, 2017, **4**, 675–682.

63 M. Jiang, J. Zhang, M. Wu, W. Jian, H. Xue, T. W. Ng, C. S. Lee and J. Xu, Synthesis of 1T-MoSe 2 ultrathin nanosheets with an expanded interlayer spacing of

1.17 nm for efficient hydrogen evolution reaction, *J. Mater. Chem. A*, 2016, **4**, 14949–14953.

64 B. Xia, T. Wang, W. Xiao, R. Zhang, P. Liu, J. Ding, D. Gao and D. Xue, Phase-transfer induced room temperature ferromagnetic behavior in 1T@2H-MoSe$_2$ nanosheets, *Sci. Rep.*, 2017, **7**, 45307.

65 J. C. Shaw, H. Zhou, Y. Chen, N. O. Weiss, Y. Liu, Y. Huang and X. Duan, *Nano Res.*, 2014, **7**, 511–517.

66 S. Upadhyay and O. P. Pandey, Synthesis of layered 2H–MoSe$_2$ nanosheets for the high-performance supercapacitor electrode material, *J. Alloys Compd.*, 2021, **857**, 157522.

67 Z. Wang, H. Y. Yue, Z. M. Yu, F. Yao, X. Gao, E. H. Guan, H. J. Zhang, W. Q. Wang and S. S. Song, One-pot hydrothermal synthesis of MoSe2 nanosheets spheres reduced graphene oxide composites and application for high performance supercapacitor, *J. Mater. Sci.: Mater. Electron.*, 2019, **30**, 8537–8545.

68 J. Shen, J. Wu, L. Pei, M. T. F. Rodrigues, Z. Q. Zhang, F. Zhang, X. Zhang, P. M. Ajayan and M. Ye, CoNi$_2$S$_4$-Graphene-2D-MoSe$_2$ as an Advanced Electrode Material for Supercapacitors, *Adv. Energy Mater.*, 2016, **6**, 1600341.

69 M. Sangeetha Vidhya, R. Yuvakkumar, P. Senthil Kumar, G. Ravi, D. Velauthapillai and M. Bijad, Recent Progression of Flower Like ZnSe@MoSe2 Designed as an Electrocatalyst for Enhanced Supercapacitor Performance, *Top. Catal.*, 2022, **65**, 684–693.

70 H. Peng, C. Wei, K. Wang, T. Meng, G. Ma, Z. Lei and X. Gong, Ni0.85Se@MoSe$_2$ Nanosheet Arrays as the Electrode for High-Performance Supercapacitors, *ACS Appl. Mater. Interfaces*, 2017, **9**, 17067–17075.

71 Y. Liu, Y. Zheng, Q. Xu, Y. Shi, Z. Tian, R. wang, G. Zhang, J. Chen, Z. Wang and W. Zheng, Controllable synthesis of NiSe/MoSe$_2$/MoO$_2$ 3D hierarchical hollow microspheres with enhanced performance for asymmetric supercapacitors, *Chem. Eng. J.*, 2020, **387**, 124121.

72 X. Gao, L. Yin, L. Zhang, Y. Zhao and B. Zhang, Decoration of NiCoP nanowires with interlayer-expanded few-layer MoSe$_2$ nanosheets: A novel electrode material for asymmetric supercapacitors, *Chem. Eng. J.*, 2020, **395**, 125058.

73 X. Chen, J. Zhu, J. Cai, Y. Zhang and X. Wang, Nanosheets assembled layered MXene/MoSe$_2$ nanohybrid positive electrode materials for high-performance asymmetric supercapacitors, *J. Energy Storage*, 2021, **40**, 102721.

74 H. Guo, J. Ning, B. Wang, X. Feng, M. Xia, D. Wang, Y. Jia, J. Zhang and Y. Hao, Sodium ion-intercalated nanoflower 1T–2H MoSe$_2$–graphene nanocomposites as electrodes for all-solid-state supercapacitors, *J. Alloys Compd.*, 2021, **853**, 157116.

75 B. Kirubasankar, P. Palanisamy, S. Arunachalam, V. Murugadoss and S. Angaiah, 2D MoSe2-Ni(OH)2 nanohybrid as an efficient electrode material with high rate capability for asymmetric supercapacitor applications, *Chem. Eng. J.*, 2019, **355**, 881–890.

76 S. S. Karade and B. R. Sankapal, Two dimensional cryptomelane like growth of MoSe2 over MWCNTs:

Symmetric all-solid-state supercapacitor, *J. Electroanal. Chem.*, 2017, **802**, 131–138.

77 J. Yu, H. Su, C. Shi, G. Qiu, L. Bai and Z. Li, Ni0. 85Se anchored on N-doped MoSe2 hybrids for long-life asymmetric supercapacitors, *Electrochim. Acta*, 2023, **471**, 143392.

78 S. Wei, C. Wan, Y. Jiao, X. Li, J. Li and Y. Wu, 3D nanoflower-like MoSe2 encapsulated with hierarchically anisotropic carbon architecture: A new and free-standing anode with ultra-high areal capacitance for asymmetric supercapacitors, *Chem. Commun.*, 2020, **56**, 340–343.

79 K. J. Huang, J. Z. Zhang and Y. Fan, Preparation of layered MoSe2 nanosheets on Ni-foam substrate with enhanced supercapacitor performance, *Mater. Lett.*, 2015, **152**, 244–247.

80 K. J. Huang, J. Z. Zhang and J. L. Cai, Preparation of porous layered molybdenum selenide-graphene composites on Ni foam for high-performance supercapacitor and electrochemical sensing, *Electrochim. Acta*, 2015, **180**, 770–777.

81 X. Liu, J. Z. Zhang, K. J. Huang and P. Hao, Net-like molybdenum selenide-acetylene black supported on Ni foam for high-performance supercapacitor electrodes and hydrogen evolution reaction, *Chem. Eng. J.*, 2016, **302**, 437–445.

82 P. Pazhamalai, K. Krishnamoorthy, V. K. Mariappan, S. Sahoo, S. Manoharan and S. J. Kim, A High Efficacy Self-Charging MoSe2 Solid-State Supercapacitor Using Electrospun Nanofibrous Piezoelectric Separator with Ionogel Electrolyte, *Adv. Mater. Interfaces*, 2018, **5**, 1800055.

83 C. Arulkumar, R. Gandhi and S. Vadivel, Ultra-thin nanosheets of $Ti_3C_2T_x$ MXene/MoSe2 nanocomposite electrode for asymmetric supercapacitor and electrocatalytic water splitting, *Electrochim. Acta*, 2023, **462**, 142742.

84 D. Zheng, G. He, Y. Mi, H. Huang Fu, Y. Li, H. Zhang, M. Wu and H. Yuan, Effect of alkaline electrolyte concentration on energy storage of core–shell structured MoSe2-PANI as supercapacitor electrode materials, *J. Mater. Sci.: Mater. Electron.*, 2023, **34**, 1734.

85 H. Mittal, A. Kumar and M. Khanuja, MoSe2-PANI Nanocomposite as Supercapacitor Electrode Material: Optimization, Mechanism and Electrochemical Performance, *ChemistrySelect*, 2022, **7**, 202201623.

86 H. Zhang, G. He, D. Zheng, H. HuangFu, Y. Li, Y. Mi, M. Wu and H. Yuan, Higher energy density of MoSe2/polyaniline capsule nanospheres for enhanced performance supercapacitor, *Nanotechnology*, 2023, **34**, 415705.

87 R. Sukanya, R. Karthik, M. Hasan, C. Breslin and J. J. Shim, Insight into the synergistic effect of 2D/2D layered metal selenides wrapped nickel boride nanoparticles based ternary heterostructure for constructing asymmetric supercapacitors with excellent energy density, *Chem. Eng. J.*, 2023, **473**, 145487.

88 S. Masanta, C. Nayak, S. Maitra, S. Rudra, D. Chowdhury, S. Raha, M. Pradhan, B. Satpati, P. Pal and A. Singha, Engineering Multifunctionality in MoSe2 Nanostructures

Via Strategic Mn Doping for Electrochemical Energy Storage and Photosensing, *ACS Appl. Nano Mater.*, 2023, **6**, 5479–5492.

89 S. Tanwar, N. Singh and A. L. Sharma, Fabrication of activated carbon coated MSe2 (M=Mo, Co, and Ni) nanocomposite electrode for high-performance aqueous asymmetric supercapacitor, *Colloids Surf., A*, 2023, **666**, 131235.

90 R. Layek, K. Mondal, S. Karmakar, R. Sarkar, D. Chattopadhyay and P. Kumbhakar, Synergistic effect in chemically synthesized noble metal nanoparticles and 2D $MoSe_2$ nanocomposite for enhanced electrochemical performance, *Mater. Today Commun.*, 2024, **38**, 108342.

91 J. Du, S. Huang, T. Xu, Y. L. Min, Y. Wang and Q. J. Xu, Facile fabrication of few-layer nanostructured $MoSe_2$ entrenched on N-doped carbon as a superior anode material for high-performance potassium-ion hybrid capacitors, *J. Alloys Compd.*, 2023, **960**, 170706.

92 X. Zhu, Z. Feng, L. Fan, Q. Wang, Y. Wei, L. Zhu, N. Li and Q. Zhang, Tailoring the morphologies of molybdenum selenides with improving their electrochemical performances for supercapacitors, *J. Energy Storage*, 2024, **89**, 111671.

93 X. He, H. Sun, Z. Li, J. Song, H. Li, C. Wang, Y. Niu and J. Jiang, Simultaneously Enhanced Energy Harvesting and Storage Performance Achieved by 3D Mix-Phase Mose2-Nise/NF, *Adv. Funct. Mater.*, 2024, **34**, 2307835.

94 K. Wang, Y. Zhou, L. Cheng, D. Li, Z. Hu, S. Chen, C. Wu, L. Song and B. Ge, Engineering Phase Transition from 2H to 1T in $MoSe_2$ by W Cluster Doping toward Lithium-Ion Battery, *Inorg. Chem.*, 2023, **62**, 21257–21264.

95 J. Yang, C. Wang, H. Ju, Y. Sun, S. Xing, J. Zhu and Q. Yang, Integrated Quasiplane Heteronanostructures of MoSe2/Bi_2Se_3 Hexagonal Nanosheets: Synergetic Electrocatalytic Water Splitting and Enhanced Supercapacitor Performance, *Adv. Funct. Mater.*, 2017, **27**, 1703864.

96 S. K. Balasingam, J. S. Lee and Y. Jun, Molybdenum diselenide/reduced graphene oxide-based hybrid nanosheets for supercapacitor applications, *Dalton Trans.*, 2016, **45**, 9646–9653.

97 M. S. Vidhya, R. Yuvakkumar, P. S. Kumar, G. Ravi, D. Velauthapillai and P. N. Asrami, Electrochemical Enhancement of Binary CuSe2@MoSe2 Composite Nanorods for Supercapacitor Application, *Top. Catal.*, 2022, **65**, 668–676.

98 J. Shui, B. Bai, X. Jiang and P. Du, High-performance MoSe2/rGO composites based on interface and phase engineering for all-solid-state symmetric supercapacitors, *Electrochim. Acta*, 2023, **469**, 143257.

99 Q. Liu, J. Ning, H. Guo, M. Xia, B. Wang, X. Feng, D. Wang, J. Zhang and Y. Hao, Tungsten-Modulated Molybdenum Selenide/Graphene Heterostructure as an Advanced Electrode for All-Solid-State Supercapacitors, *Nanomaterials*, 2021, **11**, 1477.

100 S. Tanwar, N. Singh and A. L. Sharma, Structural and electrochemical performance of carbon coated

molybdenum selenide nanocomposite for supercapacitor applications, *J. Energy Storage*, 2022, **45**, 103797.

101 P. Khichi, R. Tripathi and A. Ohlan, Optimization of synthesis parameters for molybdenum diselenide using hydrothermal method, *J. Energy Storage*, 2023, **5**, 399.

102 S. Tanwar, N. Singh, A. K. Vijayan and A. L. Sharma, Electrochemical performance investigation of different shaped transition metal diselenide materials based symmetric supercapacitor with theoretical investigation, *Surf. Interfaces*, 2023, **42**, 103504.

103 S. Tanwar, A. Arya and A. L. Sharma, MoSe$_2$-FeOOH nanocomposite as hybrid electrode material for high-performance symmetric supercapacitor, *Mater. Res. Bull.*, 2023, **160**, 112144.

104 S. Tanwar and A. L. Sharma, Aging impact on morphological and electrochemical performance of MoSe2 composite for supercapacitor application, *Ceram. Int.*, 2023, **49**, 18281–18295.

105 W. Han, L. Yuan, X. Liu, C. Wang and J. Li, Ultrathin MoSe$_2$ nanosheets decorated on carbon aerogel microspheres for high-capacity supercapacitor electrodes, *J. Electroanal. Chem.*, 2021, **899**, 115643.

106 J. Jia, J. Wu, J. Dong, Y. Tu, Z. Lan, L. Fan and Y. Wei, High-Performance Molybdenum Diselenide Electrodes Used in Dye-Sensitized Solar Cells and Supercapacitors, *IEEE J. Photovoltaics*, 2016, **6**, 1196–1202.

107 S. Upadhyay and O. P. Pandey, Effect of Se content on the oxygen evolution reaction activity and capacitive performance of MoSe$_2$ nanoflakes, *Electrochim. Acta*, 2022, **412**, 140109.

108 L. Ma, L. Xu, X. Zhou, X. Xu and L. Zhang, Synthesis of a hierarchical MoSe2/C hybrid with enhanced electrochemical performance for supercapacitors, *RSC Adv.*, 2016, **6**, 91621–91628.

109 B. He, Molybdenum diselenide nanosheets wrapping carbon aerogel nanospheres as an advanced material for supercapacitor and electrochemical sensing, *Electrochim. Acta*, 2017, **257**, 301–310.

110 M. S. Vidhya, R. Yuvakkumar, G. Ravi, B. Saravanakumar and D. Velauthapillai, Asymmetric polyhedron structured NiSe2@MoSe2 device for use as a supercapacitor, *Nanoscale Adv.*, 2021, **3**, 4207–4215.

111 H. Peng, J. Zhou, K. Sun, G. Ma, Z. Zhang, E. Feng and Z. Lei, High-Performance Asymmetric Supercapacitor Designed with a Novel NiSe@MoSe$_2$ Nanosheet Array and Nitrogen-Doped Carbon Nanosheet, *ACS Sustain. Chem. Eng.*, 2017, **5**, 5951–5963.

112 P. Pazhamalai, K. Krishnamoorthy, S. Sahoo and S. J. Kim, Two-dimensional molybdenum diselenide nanosheets as a novel electrode material for symmetric supercapacitors using organic electrolyte, *Electrochim. Acta*, 2019, **295**, 591–598.

113 S. Li, W. Zang, X. Liu, S. J. Pennycook, Z. Kou, C. Yang, C. Guan and J. Wang, Heterojunction engineering of MoSe2/MoS2 with electronic modulation towards synergetic hydrogen evolution reaction and

supercapacitance performance, *Chem. Eng. J.*, 2019, **359**, 1419–1426.

114 C. Wang, D. Wu, Y. Qin and Y. Kong, Nanowired NiMoO4/NiSe2/MoSe2prepared through in situ selenylation as a high-performance supercapacitor electrode, *Chem. Commun.*, 2021, **57**, 4019–4022.

115 D. Vikraman, S. Hussain, K. Karuppasamy, A. Feroze, A. Kathalingam, A. Sanmugam, S. H. Chun, J. Jung and H. S. Kim, Engineering the novel MoSe$_2$-Mo$_2$C hybrid nanoarray electrodes for energy storage and water splitting applications, *Appl. Catal., B*, 2020, **264**, 118531.

116 A. Alam, G. Saeed and S. Lim, One-step synthesis of 2D–2D Co (OH)$_2$–MoSe$_2$ hybrid nanosheets as an efficient electrode material for high-performance asymmetric supercapacitor, *J. Electroanal. Chem.*, 2020, **879**, 114775.

117 M. S. Vidhya, R. Yuvakkumar, P. S. Kumar, G. Ravi and D. Velauthapillai, Hydrothermal Synthesis of Flower Like MnSe2@MoSe2 Electrode for Supercapacitor Applications, *Top. Catal.*, 2022, **65**, 615–622.

118 S. Hussain, I. Rabani, D. Vikraman, T. Mehran, F. Shahzad, Y. S. Seo, H. S. Kim and J. Jung, Designing the MXene/molybdenum diselenide hybrid nanostructures for high-performance symmetric supercapacitor and hydrogen evolution applications, *Int. J. Energy Res.*, 2021, **45**, 18770–18785.

119 M. Ojha and M. Deepa, Molybdenum selenide nanotubes decorated carbon net for a high-performance supercapacitor, *Chem. Eng. J.*, 2019, **368**, 772–783.

120 J. Shen, J. Ji, P. Dong, R. Baines, Z. Zhang, P. M. Ajayan and M. Ye, Novel FeNi2S4/TMD-based ternary composites for supercapacitor applications, *J. Mater. Chem. A*, 2016, **4**, 8844–8850.

121 Y. Liu, W. Li, X. Chang, H. Chen, X. Zheng, J. Bai and Z. Ren, MoSe$_2$ nanoflakes-decorated vertically aligned carbon nanotube film on nickel foam as a binder-free supercapacitor electrode with high-rate capability, *J. Colloid Interface Sci.*, 2020, **562**, 483–492.

122 Z. Yao, C. Yu, H. Dai, J. Zhou, X. Liu and G. Sun, Hybrid fibers assembled from MoSe2/graphene heterostructures endow improved supercapacitive performance, *Carbon*, 2022, **187**, 165–172.

123 S. Singal, A. Yadav and R. K. Sharma, A high-performance asymmetric supercapacitor based on morphologically tuned CoB anode and heterostructured graphitic carbon nitride/MoSe$_2$ cathode, *J. Energy Storage*, 2024, **80**, 110300.

124 H. Guo, H. Ren, J. Tian, J. Xu, Y. Hao, L. Peng, Y. Liu and W. Yang, Polyoxometalate/MOF-derived MoSe$_2$/(Ni, Co)Se$_2$ for battery-type electrodes of high-performance supercapacitors, *J. Alloys Compd.*, 2024, **1000**, 175107.

125 L. Xu, L. Ma, T. Rujiralai, Y. Ling, Z. Chen, L. Liu and X. Zhou, Molybdenum selenide nanosheets with enriched active sites supported on titanium mesh as a superior binder-free electrode for electrocatalytic hydrogen evolution and supercapacitor, *J. Taiwan Inst. Chem. Eng.*, 2020, **107**, 35–43.

126 C. Li, Y. Zhou, P. Huo and X. Wang, Fabricated high performance ultrathin MoSe2 nanosheets grow on

MWCNT hybrid materials for asymmetric supercapacitors, *J. Alloys Compd.*, 2020, **826**, 154175.

127 M. Zhou, A. Gallegos, K. Liu, S. Dai and J. Wu, Insights from machine learning of carbon electrodes for electric double layer capacitors, *Carbon*, 2020, **157**, 147–152.

128 H. Su, S. Lin, S. Deng, C. Lian, Y. Shang and H. Liu, Predicting the capacitance of carbon-based electric double layer capacitors by machine learning, *Nanoscale Adv.*, 2019, **1**, 2162–2166.

129 X. Yang, C. Yuan, S. He, D. Jiang, B. Cao and S. Wang, Machine learning prediction of specific capacitance in biomass derived carbon materials: Effects of activation and biochar characteristics, *Fuel*, 2023, **331**, 125718.

130 S. Zhu, J. Li, L. Ma, C. He, E. Liu, F. He, C. Shi and N. Zhao, Artificial neural network enabled capacitance prediction for carbon-based supercapacitors, *Mater. Lett.*, 2018, **233**, 294–297.

131 M. Rahimi, M. H. Abbaspour-Fard and A. Rohani, A multi-data-driven procedure towards a comprehensive understanding of the activated carbon electrodes performance (using for supercapacitor) employing ANN technique, *Renew. Energy*, 2021, **180**, 980–992.

132 M. Gheytanzadeh, A. Baghban, S. Habibzadeh, A. Mohaddespour and O. Abida, Insights into the estimation of capacitance for carbon-based supercapacitors, *RSC Adv.*, 2021, **11**, 5479–5486.

133 T. D. Dongale, P. R. Jadhav, G. J. Navathe, J. H. Kim, M. M. Karanjkar and P. S. Patil, Development of nano fiber MnO2 thin film electrode and cyclic voltammetry behavior modeling using artificial neural network for supercapacitor application, *Mater. Sci. Semicond. Process.*, 2015, **36**, 43–48.

134 H. Su, C. Lian, J. Liu and H. Liu, Machine learning models for solvent effects on electric double layer capacitance, *Chem. Eng. Sci.*, 2019, **202**, 186–193.

135 J. Wang, Z. Li, S. Yan, X. Yu, Y. Ma and L. Ma, Modifying the microstructure of algae-based active carbon and modelling supercapacitors using artificial neural networks, *RSC Adv.*, 2019, **9**, 14797–14808.

136 J. Yang, A. Gallegos, C. Lian, S. Deng, H. Liu and J. Wu, Curvature effects on electric-double-layer capacitance, *China Mater.*, 2021, **31**, 145–152.

137 S. Mathew, P. B. Karandikar and N. R. Kulkarni, Modeling and Optimization of a Jackfruit Seed-Based Supercapacitor Electrode Using Machine Learning, *Chem. Eng. Technol.*, 2020, **43**, 1765–1773.

138 A. G. Patel, L. Johnson, R. Arroyave and J. L. Lutkenhaus, Design of multifunctional supercapacitor electrodes using an informatics approach, *Mol. Syst. Des. Eng.*, 2019, **4**, 654–663.

139 P. Liu, Y. Wen, L. Huang, X. Zhu, R. Wu, S. Ai, T. Xue and Y. Ge, An emerging machine learning strategy for the assisted-design of high-performance supercapacitor materials by mining the relationship between capacitance and structural features of porous carbon, *J. Electroanal. Chem.*, 2021, **899**, 115684.

140 A. Fallah, A. A. Oladipo and M. Gazi, Boron-doped sucrose carbons for supercapacitor electrode: artificial neural network-based modelling approach, *J. Mater. Sci. Mater. Electron.*, 2020, **31**, 14563–14576.

141 M. Zhou, A. Vassallo and J. Wu, Data-Driven Approach to Understanding the In-Operando Performance of Heteroatom-Doped Carbon Electrodes, *ACS Appl. Energy Mater.*, 2020, **3**, 5993–6000.

142 S. Ghosh, G. R. Rao and T. Thomas, Machine learning-based prediction of supercapacitor performance for a novel electrode material: Cerium oxynitride, *Energy Storage Mater.*, 2021, **40**, 426–438.

143 S. Parwaiz, O. A. Malik, D. Pradhan and M. M. Khan, Machine-Learning-Based Cyclic Voltammetry Behavior Model for Supercapacitance of Co-Doped Ceria/rGO Nanocomposite, *J. Chem. Inf. Model.*, 2018, **58**, 2517–2527.

144 W. A. M. Kethaki Pabasara Wickramaarachchi, M. Minakshi, X. Gao, R. Dabare and K. W. Wong, Hierarchical porous carbon from mango seed husk for electro-chemical energy storage, *Chem. Eng. J. Adv.*, 2021, **8**, 100158.

145 T. Weigert, Q. Tian and K. Lian, State-of-charge prediction of batteries and battery-supercapacitor hybrids using artificial neural networks, *J. Power Sources*, 2011, **196**, 4061–4066.

146 J. Ren, X. Lin, J. Liu, T. Han, Z. Wang, H. Zhang and J. Li, Engineering early prediction of supercapacitors' cycle life using neural networks, *Mater. Today Energy*, 2020, **18**, 100537.

147 B. Pozo, J. I. Garate, S. Ferreiro, I. Fernandez and E. Fernandez de Gorostiza, Supercapacitor electro-mathematical and machine learning modelling for low power applications, *Electronics*, 2018, **7**, 44.

148 D. Roman, S. Saxena, J. Bruns, R. Valentin, M. Pecht and D. Flynn, A Machine Learning Degradation Model for Electrochemical Capacitors Operated at High Temperature, *IEEE Access*, 2021, **9**, 25544–25553.

149 Y. Zhou, Y. Huang, J. Pang and K. Wang, Remaining useful life prediction for supercapacitor based on long short-term memory neural network, *J. Power Sources*, 2019, **440**, 227149.

150 C. Liu, Y. Zhang, J. Sun, Z. Cui and K. Wang, Stacked bidirectional LSTM RNN to evaluate the remaining useful life of supercapacitor, *Int. J. Energy Res.*, 2022, **46**, 3034–3043.

151 Y. Zhou, Y. Wang, K. Wang, L. Kang, F. Peng, L. Wang and J. Pang, Hybrid genetic algorithm method for efficient and robust evaluation of remaining useful life of supercapacitors, *Appl. Energy*, 2020, **260**, 114169.

152 C. Liu, D. Li, L. Wang, L. Li and K. Wang, Strong robustness and high accuracy in predicting remaining useful life of supercapacitors, *APL Mater.*, 2022, **10**, 061106.

153 M. Haris, M. N. Hasan and S. Qin, Early and robust remaining useful life prediction of supercapacitors using BOHB optimized Deep Belief Network, *Appl. Energy*, 2021, **286**, 116541.

154 S. Nanda, S. Ghosh and T. Thomas, Machine learning aided cyclic stability prediction for supercapacitors, *J. Power Sources*, 2022, **546**, 231975.

155 S. Mishra, R. Srivastava, A. Muhammad, A. Amit, E. Chiavazzo, M. Fasano and P. Asinari, The impact of physicochemical features of carbon electrodes on the capacitive performance of supercapacitors: a machine learning approach, *Sci. Rep.*, 2023, **13**, 6494.

156 S. Deebansok, J. Deng, E. Le Calvez, Y. Zhu, O. Crosnier, T. Brousse and O. Fontaine, Capacitive tendency concept alongside supervised machine-learning toward classifying electrochemical behavior of battery and pseudocapacitor materials, *Nat. Commun.*, 2024, **15**, 1133.

157 T. Wang, R. Pan, M. L. Martins, J. Cui, Z. Huang, B. P. Thapaliya, C. L. Do-Thanh, M. Zhou, J. Fan, Z. Yang, M. Chi, T. Kobayashi, J. Wu, E. Mamontov and S. Dai, Machine-learning-assisted material discovery of oxygen-rich highly porous carbon active materials for aqueous supercapacitors, *Nat. Commun.*, 2023, **14**, 4607.